

1  
2  
3  
4  
5  
6  
7  
8  
9  
10  
11  
12  
13  
14  
15  
16  
17  
18  
19  
20

## **Fourteen Years of Observations of the Hydrothermal System of Stromboli Volcano (Italy): Geochemical Features and Insights on the Volcanic Activity**

**Cinzia Federico<sup>1</sup>, Salvatore Inguaggiato<sup>1</sup>, Marcello Liotta<sup>1</sup>, Andrea Luca Rizzo<sup>2</sup> and Fabio Vita<sup>1</sup>**

<sup>1</sup>Istituto Nazionale di Geofisica e Vulcanologia, Sezione di Palermo, Via Ugo La Malfa, 153 - 90146 Palermo, Italy

<sup>2</sup>Istituto Nazionale di Geofisica e Vulcanologia, Sezione di Milano, Via Alfonso Corti, 12 - 20133 Milano, Italy.

Corresponding author: Salvatore Inguaggiato ([salvatore.inguaggiato@ingv.it](mailto:salvatore.inguaggiato@ingv.it))

### **Key Points:**

- The composition of water and dissolved gases results from the mixing of meteoric and marine water and the input of volcanic gases
- ~~Variations are~~ due to the extent of mixing, the solubility-driven fractionation of dissolved gas species, ~~the~~ volcanic activity
- The gas dissolved in the aquifer has a  $^3\text{He}/^4\text{He}$  range of 3.-4.5 Ra, similar to that measured in olivines and pyroxenes.

## 21 Abstract

22 In active volcanoes, magmatic fluids rising toward the surface may interact with shallow  
23 waters, thereby favoring the formation of hydrothermal systems that, therefore, are supposed to  
24 record variations of the magmatic dynamics at depth. Here, we report on a dataset on the  
25 chemical and isotopic composition of thermal waters and dissolved gases from Stromboli Island  
26 (Aeolian Volcanic Arc, Southern Italy) that globally span fourteen years (2004-2018) of  
27 continuous observations.

28 We show that the shallow thermal aquifer of Stromboli results from variable mixing proportions  
29 between meteoric water, seawater, and magmatic fluids; gas-water-rock interactions occur,  
30 which induce a large spectrum of variations in both water and gas chemistry. These processes  
31 apparently do not affect the  $^3\text{He}/^4\text{He}$  of helium dissolved in thermal waters, which has a  
32 magmatic signature that varies in response to changes in magmatic dynamics at depth. By also  
33 considering previous investigations, we pointed out that, in periods of more intense activity, the  
34 helium isotopes approached the signature of the gas emitted from the magma residing at 7-10 km  
35 depth.

36 We ultimately propose an interpretative model that reconstructs the complex processes occurring  
37 in the hydrothermal system, which is rooted below sea level and next to the main conduits.

38 We conclude by noting that the investigation of hydrothermal waters in active volcanoes is a  
39 promising tool to examine magmatic fluids and their shallow circulation, as well as for  
40 evaluating the state of activity of a volcano, especially when summit areas are inaccessible.

41

## 42 1 Introduction

43 Hydrothermal systems usually form in active volcanoes as a result of the condensation of  
44 a saline liquid phase upon decompression of H<sub>2</sub>O-rich fluids degassed from magma or by  
45 absorption of HCl-rich and SO<sub>2</sub>-rich fluids in aquifers fed by meteoric or seawater and the  
46 contact of these acidic and hot fluids with the surrounding rocks (Webster and Manderville,  
47 2007). The shallowest level of hydrothermal systems is often heated by the acidic vapor  
48 separated from deeper aquifers. Gas-water-rock interactions occur and trigger a set of chemical-  
49 physical processes and reactions that often lead to significant changes in the pristine composition  
50 of magmatic fluids. Hydrothermal systems can be found in many volcanoes on Earth,  
51 irrespective of the geodynamic setting of formation, as they form in open- or closed-conduit  
52 volcanoes, in subaerial or submarine conditions, and consist of one or two phases (liquid and/or  
53 vapor) developed into convective fluid cells (Chiodini et al., 1995, 2001, 2005; Osinski et al.,  
54 2001; Finizola et al., 2002; Caliro et al., 2004, 2007; Lupton et al., 2008; Antoine et al., 2009;  
55 Federico et al., 2010; Taran et al., 2017; Mauri et al., 2018; Rizzo et al., 2019). Hydrothermal  
56 systems dissipate much of the energy produced by the volcano and may display the first  
57 indications of impending crises (e.g., Chiodini et al., 2016). The nature and extent of  
58 hydrothermal systems (Revil and Linde, 2006; Finizola et al., 2009, Revil et al., 2011; Lénat et  
59 al., 2012; Mauri et al., 2018) influence the occurrence of hazards such as phreatic and  
60 phreatomagmatic explosions, and flank collapses (Lorenz and Kurszlaukis, 2007; Weinsten,  
61 2007). Similarly, the geochemical characterization and monitoring of hydrothermal fluids are of  
62 great importance to constrain i) the composition, temperature, pressure, and redox conditions of  
63 the system, ii) the state of activity of the volcano, iii) the evolution of unrest, particularly in those

64 systems where access to high-temperature fumaroles is unsafe (Giggenbach, 1975; Chiodini et  
65 al., 1995, 2001, 2005; Caliro et al., 2004, 2007; Capasso et al., 1999; 2005; Inguaggiato et al.,  
66 2000, 2004, 2005, 2010; Lupton et al., 2008; Federico et al., 2010; Rizzo et al., 2015, 2019;  
67 Taran et al., 2017; Mauri et al., 2018). In many cases, the shallow fluids of meteoric or marine  
68 origin feeding the volcanic aquifers may modify the pristine signature of the deep fluids and the  
69 signals linked to volcanic activity. Understanding gas–water interaction processes, which modify  
70 the pristine physicochemical characteristics of fluids, sheds light on both the origin of the fluids  
71 and the degree of this interaction at depth. In recent years, the study of the volatiles dissolved in  
72 the thermal waters of several volcanic systems has provided useful ~~indications on~~ the origin of  
73 these fluids and the processes ~~able to~~ modify their chemical and isotope composition during their  
74 ~~pathway~~ toward the surface (Inguaggiato et al., 2000; 2005; 2010; Capasso et al., 2005; Paonita  
75 et al., 2016; Federico et al., 2017a).

76 Stromboli Island (Aeolian Volcanic Arc, Italy) is an open-conduit volcano characterized by  
77 persistent explosive activity, which makes the regular monitoring of fumarole gases in the crater  
78 area hazardous (Carapezza and Federico, 2000; Capasso et al., 2005; Rizzo et al., 2009). ~~Instead,~~  
79 the thermal aquifer identified at the base of the subaerial part of the edifice (Carapezza and  
80 Federico, 2000; Finizola et al., 2002, 2003, 2009; Capasso et al., 2005; Revil et al., 2011)  
81 represents a safe point of observation to acquire insights on the volcano-hydrothermal system.

82 Many geochemical studies on the thermal aquifer, which is ~~generally~~ accessible via privately  
83 drilled wells, have been carried out in the last two decades (Carapezza and Federico, 2000;  
84 Carapezza et al., 2004; Inguaggiato and Rizzo, 2004; Capasso et al., 2005; Liotta et al., 2006;  
85 Federico et al., 2008; Grassa et al., 2008; Rizzo et al., 2008, 2009, 2015; Madonia et al., 2021).  
86 These studies revealed i) the main composition of thermal waters and gases dissolved therein, ii)  
87 the influence of shallow marine and meteoric waters on the hydrothermal composition, iii) the  
88 presence and extent of gas-water-rock interaction processes, and iv) a magmatic signature  
89 concerning helium isotopes. These studies brought an invaluable understanding of fluid  
90 geochemistry at Stromboli, but most of them took place over short periods, often limited to  
91 single effusive eruptions.

92 In this work, we report on the chemical and isotopic composition of thermal waters and dissolved  
93 gases from Stromboli Island, ~~which~~ cover fourteen years of observations from 2004 to 2018. We  
94 characterize the hydrothermal system of Stromboli, highlighting the main processes occurring  
95 therein. The aim is to provide an interpretative framework ~~of~~ the variations in water and gas  
96 chemistry, which ~~takes into account~~ the ~~different~~ processes ~~related to~~ meteoric input, seawater  
97 contamination, gas-water-rock exchanges, and water mixing, before relating them to  
98 volcanological processes. We report on 8 thermal water wells located in the area of Stromboli  
99 village ~~for a total of~~ 112 sampling campaigns. We show that ~~the~~ magmatic fluids re-equilibrate at  
100 hydrothermal conditions and the gases collected in the monitored wells show variable relative  
101 contents of CO<sub>2</sub>, He, and CH<sub>4</sub>, the latter being of hydrothermal origin. The variable extent of  
102 rock-leaching and seawater/meteoric mixing modulate the chemistry and isotopic ratios of the  
103 shallow water. The dissolved gas shows a magmatic signature of <sup>3</sup>He/<sup>4</sup>He, comparable to that  
104 measured in olivine and pyroxene minerals (Martelli et al., 2014), whose temporal monitoring  
105 revealed systematic variations during ~~the recorded~~ effusive eruptions and ~~main~~ phases of ~~high~~  
106 volcanic activity.

107

## 108 2 Study area

### 109 2.1 Volcanological background of Stromboli

110 Stromboli Island is an active volcano ~~belonging to~~ the Aeolian Archipelago (Italy), which  
111 is located in the southeastern Tyrrhenian Sea (Figure 1), and associated with the Quaternary  
112 subduction of the African plate below the European plate (e.g., Gasparini et al., 1982). Stromboli  
113 was built ~~up~~ on a 17 km-thick continental crust (Morelli et al., 1975; Panza et al., 2007) and is  
114 characterized by persistent explosive activity from the summit craters (usually every 10-20 min),  
115 known throughout the world as “Strombolian Activity” (e.g., Rosi et al., 2000). This Strombolian  
116 activity is occasionally interrupted by lava effusions and/or violent explosions referred to as  
117 “major explosions” and “paroxysms”, which eject large bombs and may occasionally cause hot  
118 avalanches, landslides, and ~~ultimately also~~ tsunamis. In the last 35 years, four effusive eruptions  
119 occurred, ~~in~~ 1985, 2002, 2007, and 2014 (Inguaggiato et al. 2018), ~~in~~ addition to many major  
120 explosions and lava overflows. Paroxysmal explosions were recorded in 2003, 2007, and two in  
121 2019 (Andronico et al., 2021).

122 Stromboli erupts magmas belonging to four distinct series, i.e. calc-alkaline (CA), high  
123 potassium calc-alkaline (HKCA), shoshonitic (SHO), and potassic (KS) (e.g., Francalanci et al.,  
124 1988, 1989). All erupted magmas are mafic ( $\text{SiO}_2 < 55\%$ ,  $\text{MgO} > 4\%$ ) and exhibit similar  
125 subduction-related patterns of trace elements (Francalanci et al., 1993, 2007; Tommasini et al.,  
126 2007). The geochemical signature of the primitive batches of the Stromboli magmatic series  
127 (CA, HKCA, SHO, KS) is attributed to the partial melting of a mantle wedge, made  
128 heterogeneous by the variable metasomatism by fluids released by the subducting slab  
129 (Tommasini et al., 2007; Schiavi et al., 2012). Moreover, crustal contamination likely occurred  
130 in the KS magmas (Ellam et al., 1989; Francalanci et al., 1993, 2004; Tommasini et al., 2007;  
131 Schiavi et al., 2012; Martelli et al., 2014).

132 The present-day activity of Stromboli belongs to the shoshonitic series and consists of two types  
133 of magmas: i) a high porphyritic (HP) volatile-poor magma, stored at 2-4 km depth ~~bsl~~ that  
134 undergoes slow but continuous degassing-induced crystallization and ii) a low porphyritic (LP)  
135 volatile-rich magma stored at 7-10 km depth ~~bsl~~, refilled by  $\text{CO}_2$ -rich magmas rising from the  
136 mantle (e.g., Francalanci et al., 2004; Bertagnini et al., 2008; Métrich et al., 2010; 2021). The  
137 persistent Strombolian activity of the volcano is maintained in a steady state, driven by the  
138 continuous refilling of the shallow magmatic reservoir with deep volatile-rich magmas, together  
139 with almost continuous magma emission during ordinary activity (e.g., Landi et al., 2009;  
140 Métrich et al., 2010). Magmatic volatiles, which represent the engine of the explosive volcanic  
141 activity, are largely emitted from the summit craters during both quiescence and eruptive phases,  
142 but they also escape from the soil in the summit area and along the upper flanks of the edifice,  
143 and at the base of the cone, focused along tectonic lineaments (Carapezza and Federico, 2000;  
144 Finizola et al., 2006; Carapezza et al., 2009; Inguaggiato et al., 2019; 2020; 2021).


145

## 146 2.1 The Stromboli thermal aquifer

## 147 2.2.1 Hydrogeology

148 Previous hydrogeological studies (Revil et al. 2011; Madonia et al. 2021)  
149 described the characteristics of the aquifer in this sector of Stromboli. Based on electrical  
150 resistivity measurements, soil CO<sub>2</sub> concentrations, temperature, and self-potential  
151 measurements, Revil et al. (2011) provided insights regarding the position of shallow  
152 aquifers and the extension of the hydrothermal system. They found that ~~the~~ self-potential  
153 data reveal the position of an unconfined aquifer above the villages of Scari and San  
154 Vincenzo and provided an estimate of the depth of this aquifer. More recently, Madonia  
155 et al. (2021) indicated that there is a unique groundwater body in the form of a thin lens  
156 of fresh water, floating above the infiltrating seawater and suggested the existence of a  
157 multi-level aquifer, ~~according to the presence~~ of alternating lavas and pyroclastic  
158 deposits.

## 159 2.2.2 Chemistry of groundwater

160 The thermal waters were studied by Carapezza and Federico (2000), Carapezza et  
161 al. (2004), Capasso et al. (2005), and Grassa et al. (2008). The authors found that the  
162 chemical composition of thermal waters is the result of mixing in different proportions  
163 between seawater and meteoric water, heated by vapor ascending from depth, with  
164 limited interaction with the volcanic rocks. They reported temperatures in the range of  
165 35–47°C, water table at depths of 5–20 m b.g.l., and a wide range of dissolved salt  
166 content ranging from 8,200 to 40,000 mg/L, as the result of variable fractions of  
167 seawater. The reported average pH values were in the range of 6.31 and 6.97. The  
168 chemical composition of both end-members is modified by the dissolution of a CO<sub>2</sub>-rich  
169 gas phase and by leaching of the aquifer-hosting rocks. Liotta et al. (2006) also studied  
170 the chemical composition of the rainwater which is mainly controlled by the contribution  
171 of ~~the~~ marine aerosol near the coast, whereas it is strongly influenced by volcanic activity  
172 near the summit vents. The hydrogen and oxygen isotopic composition of rainfall shows  
173 seasonal variability and correlates with air temperature, while deuterium excess values  
174  show a positive correlation with altitude. The isotope composition of the meteoric  
175 recharge was retrieved from the mean annual volume-weighted values, being between -  
176 6.2 and -8.4‰ for δ<sup>18</sup>O and between -35 and -45‰ for δD (versus the Vienna Standard  
177 Mean Ocean Water, V-SMOW) (Liotta et al. 2006).

## 178 2.2.3 Chemistry and carbon isotopes of dissolved gas

179 The chemical and isotope composition of ~~the~~ dissolved gas in the Stromboli  
180 shallow aquifer was discussed by Capasso et al. (2005) and Federico et al. (2008). The  
181 air-free composition of the dissolved gas is dominated by CO<sub>2</sub>, with variable ~~contents~~  
182 of He and CH<sub>4</sub>. While the authors claim a magmatic origin for both CO<sub>2</sub> and He, the CH<sub>4</sub>  
183 contents were ascribed to a contribution of fluids from a hydrothermal system.

184 A wide compositional variability characterizes both the whole aquifer and each sampling  
 185 site (Capasso et al., 2005; Federico et al., 2008). This variability was ascribed to the  
 186 heterogeneity of volcanic deposits, made of alternating levels of pyroclastics of different  
 187 grain sizes, porosity, and permeability, which host small water bodies variably  
 188 contaminated by seawater and volcanic fluids. The variable enrichment in He and CH<sub>4</sub>  
 189 compared to an original CO<sub>2</sub>-dominated volcanic gas could be a consequence of  
 190 modification of the gas during dissolution in the aquifer. Both vapor separation from a  
 191 hydrothermal aquifer and dissolution in the shallow meteoric aquifer would promote the  
 192 preferential partitioning of the less-soluble gas species into the vapor phase, namely He  
 193 and CH<sub>4</sub> compared to CO<sub>2</sub>, and also the isotope fractionation of gaseous CO<sub>2</sub> compared to  
 194 dissolved carbon species (Capasso et al., 2005; Federico et al., 2008).

195 Some of the variability in the ~~observed data~~ was also ascribed to the changeable input of  
 196 volcanic fluids over time. Carapezza et al. (2004) and Capasso et al. (2005) reported on  
 197 significant variations in the chemical and isotopic composition of CO<sub>2</sub> in all the  
 198 monitored thermal wells ~~by the time of the effusive eruption that occurred in the 2002-~~  
 199 ~~2003 period~~. Values of dissolved CO<sub>2</sub> as high as 75-220 cc/L at STP in March-July 2002  
 200 were measured six months before the onset of the eruption, which was shortly preceded  
 201 by ~~one~~ order of magnitude increase in the soil CO<sub>2</sub> flux in the summit area (Inguaggiato  
 202 et al., 2011). Moreover, before the 5 April 2003 paroxysm, Carapezza et al. (2004) and  
 203 Rizzo et al. (2008) observed a marked decrease in the pH values of 0.1-0.5 pH units in  
 204 the thermal water wells located in the Stromboli village, ascribed to the increased input of  
 205 CO<sub>2</sub> in the shallow thermal aquifer.

206 Inguaggiato et al. (2017a,b) reported on variations in pCO<sub>2</sub> in two wells for a limited  
 207 period, related to variations in soil CO<sub>2</sub> fluxes recorded both in Scari (~~str01~~, Inguaggiato  
 208 et al., 2017b) and at the summit of the volcano in the same period (Inguaggiato et al.,  
 209 2017a).

#### 210 2.2.4 Noble gases

211 Carapezza and Federico (2000) ~~were the first to report~~ on the noble gas  
 212 composition (concentration of <sup>4</sup>He and <sup>20</sup>Ne, <sup>4</sup>He/<sup>20</sup>Ne and <sup>3</sup>He/<sup>4</sup>He) of fluids from  
 213 Stromboli in a fumarole located at Pizzo Sopra La Fossa (Figure 1), called SC5. This  
 214 fumarole was monitored from 1992 to 1998 and showed <sup>3</sup>He/<sup>4</sup>He values in the range of  
 215 2.71-3.55 R<sub>a</sub>, indicating a clear magmatic signature. However, the gases showed a  
 216 variable but significant air contamination, as suggested by <sup>4</sup>He/<sup>20</sup>Ne between 1.0 and 3.2,  
 217 implying an uncertainty in the corrected <sup>3</sup>He/<sup>4</sup>He values. Carapezza and Federico (2000)  
 218 evidenced that the <sup>3</sup>He/<sup>4</sup>He values measured at SC5 were appreciably lower than those  
 219 measured at Vulcano Island and Mt Etna, inferring a contribution of radiogenic crustal  
 220 <sup>4</sup>He to the local fumarolic gas.

221 For the first time in 2002, Inguaggiato and Rizzo (2004) studied the noble gas  
 222 composition of thermal waters from Stromboli within a methodological study aimed at  
 223 developing and consolidating a technique to determine and monitoring ~~ing of~~ the isotope  
 224 ratio of dissolved He in groundwater. Three wells were selected (Cusolito, Fulco, and  
 225 Zurro; Figure 1) where water samples were collected. Helium concentrations were in the

226 range of  $1.4\text{--}6.2 \cdot 10^{-4}$  cc/L at STP, in the same order of magnitude as that measured by  
 227 Carapezza and Federico (2000). Neon concentrations ranged between  $3.5 \cdot 10^{-5}$  and  $1.6 \cdot 10^{-5}$   
 228  $\text{cc/l}$  at STP. The  $^4\text{He}/^{20}\text{Ne}$  was 3.7–9.6. The  $^4\text{He}/^{20}\text{Ne}$  corrected for air contamination  
 229 ( $R_c/R_a$ ) was in the range of 4.06–4.23  $R_a$ .

230 Inguaggiato and Rizzo (2004) found  $^3\text{He}/^4\text{He}$  values of 4.06–4.23  $R_a$  in thermal waters  
 231 sampled at the base of the subaerial volcanic edifice. To explain the lower isotopic  
 232 signature of SC5, they argued that the water-rock interaction in a hydrothermal system  
 233 recognized in the summit area by Finizola et al. (2002, 2003) could enhance the  
 234 contribution of radiogenic  $^4\text{He}$  from U and Th decay, thus decreasing the pristine  $^3\text{He}/^4\text{He}$   
 235 in Pizzo Sopra La Fossa fumaroles. Finally, Inguaggiato and Rizzo (2004) highlighted  
 236 that the study of dissolved gases in the thermal waters in Stromboli could be strategic for  
 237 monitoring purposes, besides validating the technique for the determination of dissolved  
 238 noble gases.

239 Between 2002 and 2014, Capasso et al. (2005) and Rizzo et al. (2009, 2015) reported on  
 240 the first dataset of noble gas monitoring in thermal waters collected with a roughly  
 241 monthly frequency. During that period of monitoring, i) an effusive eruption occurred at  
 242 Stromboli in 2002-2003 as well as a paroxysmal explosion on 5 April 2003; ii) an  
 243 effusive eruption occurred in February-April 2007, including a paroxysmal explosion that  
 244 occurred on the 15<sup>th</sup> March, iii) an effusive eruption occurred in August-November 2014.

245 The above-reported studies on time series found that  $^3\text{He}/^4\text{He}$  values ranged from 3.4 and  
 246 4.5  $R_a$ , with slight or negligible differences among the wells, while the  $^4\text{He}/^{20}\text{Ne}$  was in  
 247 the range of 1-11. These values were comparable to those found by Inguaggiato and  
 248 Rizzo (2004), except for the natural variability related to the persistent activity of  
 249 Stromboli. In addition, Capasso et al. (2005) showed that the  $^3\text{He}/^4\text{He}$  measured in the  
 250 thermal waters were comparable to the unique value of 4.3  $R_a$  found during the eruption  
 251 in newly-formed fumaroles located close to the north-east crater (Finizola and Sortino,  
 252 2003; Finizola et al., 2002). This evidence further confirmed that the range of  $^3\text{He}/^4\text{He}$   
 253 values found in thermal waters is representative of the magmatic signature and can be  
 254 used for evaluating the state of activity of the volcano. In terms of application to volcano  
 255 monitoring, Capasso et al. (2005) and Rizzo et al. (2009; 2015) showed that the temporal  
 256 variations of  $^3\text{He}/^4\text{He}$  occurred simultaneously in all the thermal water wells. Importantly,  
 257 the highest  $^3\text{He}/^4\text{He}$  values (4.50–4.56  $R_a$ ) were always measured during the eruptive  
 258 phases. These high values were interpreted as due to new input of undegassed LP-like  
 259 magma and the transfer of its gas towards the surface. After the eruptive phases, different  
 260 pulses of magma input were hypothesized for a few weeks, as indicated by relatively high  
 261  $^3\text{He}/^4\text{He}$  values at all the sampling sites, suggesting the resumption of the Strombolian  
 262 activity (Capasso et al., 2005; Rizzo et al., 2009; 2015).

263 Martelli et al. (2014) studied the elemental (He, Ne, and Ar) and isotopic (He and Ar)  
 264 compositions of fluid inclusions hosted in olivine and clinopyroxene from lavas,  
 265 pyroclastics, and cumulate xenoliths erupted by Stromboli in the last 60 ka. The authors  
 266 found that most of the investigated samples exhibit a  $^3\text{He}/^4\text{He}$  ratio in the range of 4.0–  
 267 4.9  $R_a$ , with only the minerals of the KS series showing lower isotopic values ( $\leq 3.5 R_a$ ).

268 This variability was interpreted as due to a heterogeneous mantle source. In detail, the  
269 maximum  $^3\text{He}/^4\text{He}$  ratio found in the LP fluid inclusions (i.e., 4.6 Ra) corresponds to the  
270 maximum ratio measured in the hydrothermal fluids (Capasso et al., 2005; Rizzo et al.,  
271 2009), suggesting that this value can be considered as a marker of the maximum  
272 contribution from the LP magma in surface gases.

273

### 274 **3 Materials and Methods**

#### 275 3.1 Sampling and in situ measurements

276 Most of the sampling sites are wells located on the northeast side of Stromboli  
277 Island (Figure 1), drilled for private use. Limoneto and COA wells were drilled for purely  
278 scientific use aimed at groundwater monitoring. We will also report and discuss data  
279 relative to two samples of dripping water from a cave in the neighborhood of Fulco well  
280 (FCDW) that we consider representative of the infiltrating water of that area. The highest  
281 piezometric level (0.86 m asl) is measured in the COA well, the farthest from the coast,  
282 whereas in the other wells, closer to the coast, a piezometric level of around 0.5 m is  
283 measured, with a hydraulic gradient of  $1.7 \text{ m km}^{-1}$  at COA and  $2.0 \text{ m km}^{-1}$  at Limoneto.  
284 Groundwater monitoring was performed by using portable equipment, an electric  
285 submersible pump, or on-site plumbing when present. The chemical-physical parameters  
286 (pH, temperature, electrical conductivity, and Redox potential) were measured in the field  
287 using Orion Star A series instruments, equipped with Hamilton electrodes. At the  
288 beginning of each sampling activity, the pH-meter was calibrated using at least two  
289 buffers. Over the sampling period, the calibration of the pH-meter was verified between  
290 one sampling and another by a single-point calibration at pH 7. Calibration of the  
291 conductivity meter Orion Star A 122 was performed using the standard of a known  
292 concentration that is close to the expected range of conductivity of the water being  
293 sampled. The same sampling procedure was used over the entire study period. A  
294 submersible pump was placed approximately in the mid-portion of the water column in  
295 the wells and switched on for a sufficient duration (15-30 min) to purge the well of the  
296 stagnant water, before the sampling. During this stage, pH, electrical conductivity, and  
297 turbidity of the water were monitored in order to verify the achievement of adequate  
298 purging. Adequate purging is achieved when the pH and electrical conductivity of the  
299 water show constant values, and the turbidity has disappeared, resulting in water  
300 clarification. The condition of stability requires pH variations within 0.1 unit and  
301 conductivity variations within about 5%.

302 For the determination of dissolved major ions, water samples were filtered with  $0.45 \mu\text{m}$   
303 filters and stored in LD-PE (low-density polyethylene) bottles. The aliquots to be  
304 analyzed for cation content were also acidified to  $\text{pH} \approx 2$  with Suprapur(R)  $\text{HNO}_3$ . The  
305 alkalinity was determined by titration with  $\text{HCl}$  (0.1 N) on an untreated aliquot.

306 Water samples, used for dissolved gas and isotope determinations, were collected in  
307 serum bottles and sealed underwater with Teflon-faced rubber septa and aluminum seals,  
308 to minimize atmospheric contamination. Glass bottles were filled while avoiding



309 turbulent water flow, by keeping the pump flow rate low. In addition, silicon tubes were  
310 inserted directly down to the bottom of the serum bottle while it is immersed in a basin  
311 filled with the same water to be sampled (Liotta and Martelli, 2012). The bottles were  
312 sealed by crimping the Teflon-faced rubber septum using an aluminum seal.

### 313 3.2 Chemical and isotopic analyses

314 Major elements were analyzed in the laboratory of INGV-Palermo using ion  
315 chromatography systems (Dionex-Thermo ICS 1100) in suppressed mode, equipped with  
316 a column AS14A and a precolumn (AG14A) for anions ( $F^-$ ,  $Cl^-$ ,  $Br^-$ , and  $SO_4^{2-}$ ), and a  
317 column CS12A and precolumn CG12A for cations ( $Li^+$ ,  $Na^+$ ,  $K^+$ ,  $Mg^{++}$ , and  $Ca^{++}$ ). The  
318 columns work under a continuous flow of a carbonate–bicarbonate eluent for anions and  
319 a methanesulfonic acid eluent for cations. The precision and accuracy of the method are  
320 described in Prano and Liotta (2018) and are usually below 5%. During each analytical  
321 session, a certified material was analyzed to check the accuracy.

322 Dissolved gases were sampled and analyzed according to the method described by  
323 Capasso and Inguaggiato (1998), which is based on the equilibrium partition of gas  
324 species between a liquid and a gas phase after the introduction of a host gas (Ar) into the  
325 sample.

326 The analysis was performed in the INGV-Palermo laboratories using a gas  
327 chromatograph (Perkin Elmer Clarus 500) equipped with a double detector (a thermal  
328 conductivity detector [TCD] and a flame ionization detector [FID] with a methanizer) and  
329 Ar as the carrier gas.  $H_2$ ,  $O_2$ ,  $N_2$ , and  $CO_2$  were measured using the TCD detector, while  
330  $CH_4$  and  $CO$  were determined using the FID detector coupled to the methanizer (Capasso  
331 and Inguaggiato, 1998). Standard mixtures are routinely analyzed before any analytical  
332 session, and the analytical precision was always better than 5%.

333 The isotope analyses were performed in the laboratories of INGV-Palermo.

334 A completely automated procedure was used to determine the  $\delta^{13}C$  of total dissolved  
335 inorganic C (TDIC) in water ( $\delta^{13}C_{TDIC}$ ) (Capasso et al., 2005). C-isotope ratios ( $^{13}C/^{12}C$ )  
336 were measured using a mass spectrometer (Delta V Plus) connected online to the  
337 GasBench II system. The results were reported in  $\delta\%$  versus the V-PDB standard, with a  
338 precision better than  $\pm 0.1\%$ .

339 The analysis of He and Ne concentrations,  $^3He/^4He$ , and  $^4He/^{20}Ne$  of the gases dissolved  
340 in thermal waters was performed in the laboratories of INGV-Palermo (Vita et al., 2023).

341 Noble gases were extracted from the water following the method developed by  
342 Inguaggiato and Rizzo (2004). ~~This method uses the same theoretical principle as that~~  
343 ~~proposed by Capasso and Inguaggiato (1998) for the study of gases dissolved in water,~~  
344 ~~but it was optimized for helium and neon isotopic measurements. Therefore, two distinct~~  
345 aliquots of water samples were sampled. After introducing the extracted gases in a system  
346 of ultra-high-vacuum purification lines,  $^3He$ ,  $^4He$ , and  $^{20}Ne$  and the  $^4He/^{20}Ne$  ratios were  
347 determined by separately admitting He and Ne into a split flight tube mass spectrometer  
348 (GVI-Helix SFT, for He analysis) and a multi-collector mass spectrometer (Thermo-

Helix MC plus, for Ne analysis). He and Ne purification and separation were carried out based on standard purification procedures (Rizzo et al., 2015; 2016).  $^3\text{He}/^4\text{He}$  ratio is expressed as  $R/R_a$  ( $R_a$  being the He isotope ratio of air and equal to  $1.39 \cdot 10^{-6}$ ), and the analytical error is generally below 0.7%. The  $^3\text{He}/^4\text{He}$  values were corrected for the atmospheric contamination based on the measured  $^4\text{He}/^{20}\text{Ne}$  ratio, as follows:

$$R_c/R_a = \left[ R_M/R_a \left( \frac{^4\text{He}}{^{20}\text{Ne}} \right)_M - \left( \frac{^4\text{He}}{^{20}\text{Ne}} \right)_A \right] / \left[ \left( \frac{^4\text{He}}{^{20}\text{Ne}} \right)_M - \left( \frac{^4\text{He}}{^{20}\text{Ne}} \right)_A \right] \quad 1$$

where subscripts M and A refer to measured and ASW theoretical values, respectively [ $(^4\text{He}/^{20}\text{Ne})_A=0.285$ ]. The corrected  $^3\text{He}/^4\text{He}$  ratios reported in the text and Table 1 are expressed as  $R_c/R_a$  values.

358

## 359 4 Results

### 360 4.1 Chemistry of groundwater

361 The whole dataset covers the period 2004 – 2018 and includes data relative to the wells  
 362 ~~named~~ Fulco, Cusolito, Zurro, Limoneto, Ossidiana, Saibbo, COA, and Piscità (All the  
 363 data produced in this work have been archived in the EarthChem data repository, Vita et  
 364 al. 2023). We also report and discuss the geochemical data relative to two samples of  
 365 dripping water from a cave in the neighborhood of Fulco well (FCDW, Fulco Cave  
 366 Dripping Water) that we consider representative of the infiltrating water in that area. The  
 367 water temperature is almost constant over time at each site (as previously observed by  
 368 Grassa et al, 2008): mean values 35.8°C at Zurro, 41.5°C at Fulco, 40.1°C at Saibbo,  
 369 40.1°C at Limoneto, 41.9°C at COA, 42.8°C at Cusolito, 34.8°C at Ossidiana, and 32.7°C  
 370 at Piscità. The pH values range between 5.72 and 7.43 and are systematically lower at  
 371 COA, Saibbo, and Fulco sites, with average values of 6.33, 6.33, and 6.39, respectively.  
 372 All the other sites exhibit higher average pH values: 6.70 at Cusolito, 6.75 at Limoneto,  
 373 6.93 at Ossidiana, 6.86 at Zurro, and 7.11 at Piscità. All the samples fall around the line  
 374 representative of the Na/Cl ratio in seawater, between the FCDW sample and the  
 375 Mediterranean seawater composition (Figure 2) (Grassa et al., 2008; Carapezza and  
 376 Federico, 2000; Carapezza et al., 2004; Capasso et al., 2005). When taking into account  
 377 the isotope composition of thermal waters, all the samples fall between the meteoric end-  
 378 member and seawater (Figure 3).

379

### 380 4.2 Chemistry and carbon isotopes of the dissolved gas

381 We present the dissolved gas composition and carbon isotope composition of dissolved  
 382 carbon (Vita et al. 2023).

383 The ~~average composition of the~~ dissolved gas is dominated by  $\text{CO}_2$  in all wells, whose  
 384 contents range from 1.5 to 290 cc/L at STP. Nitrogen contents range from 3 to 23 cc/L at  
 385 STP, whereas dissolved  $\text{O}_2$  was always below the concentration of air-saturated water (7

386 cc/L at STP) with  $N_2/O_2$  ratios much higher than in air-saturated water at STP ( $N_2/O_2 \sim$   
387 2). The  $CH_4$  contents range from  $1 \cdot 10^{-4}$  to  $5 \cdot 10^{-2}$  cc/L at STP.

388 The triangular diagram of Figure 4 shows a wide variation in the relative proportions of  
389 He,  $CO_2$ , and  $CH_4$  in the dissolved gas phase, in both the whole aquifer and each sampled  
390 well. In particular, Fulco and Ossidiana wells are characterized, on average, by the  
391 highest relative contents of  $CO_2$ , although some samples from both wells point towards  
392 the  $CH_4$  corner. The wells COA, Cusolito, and Zurro show a stronger enrichment in both  
393 He and  $CH_4$ , with few samples pointing to the  $CH_4$  corner. Lastly, Limoneto and Piscit a  
394 are characterized by the most evident enrichment in He.

395 The Stromboli thermal aquifer is characterized by a wide range of  $CO_2$  contents,  
396 observed even in wells located in a restricted area and, in some cases, in a given well  
397 over time. The high  $CO_2$  contents in the aquifer are matched by correspondingly more  
398 positive values of the isotope composition of the dissolved  $CO_2$  ( $\delta^{13}C_{CO_2}$ , Vita et al.,  
399 2023), computed from the measured  $\delta^{13}C_{TDC}$  (Vita et al., 2023). The pristine isotope  
400 composition of gaseous  $CO_2$  is retrieved from the measured  $\delta^{13}C_{TDC}$  by applying the  
401 fractionation factor between total dissolved carbon (TDC) and gaseous  $CO_2$  ( $\alpha_{TDC-CO_{2,g}}$ ),  
402 computed according to the weighted contribution of the enrichment factors  $\epsilon$  between  
403  $CO_2$  and each dissolved carbon species, as described by Capasso et al. (2005) and  
404 Federico et al. (2008). As observed in the graph, the highest dissolved  $CO_2$  contents,  
405 measured in Fulco well, are associated with values of  $\delta^{13}C_{CO_2}$  of about -1.5 ‰. The  
406 lowest  $CO_2$  contents, characterized by relatively more negative  $\delta^{13}C_{CO_2}$  values, were  
407 measured in the wells Piscit a and Zurro.

### 408 4.3 Chemistry of noble gases

409 Here, we integrate the existing data on He and Ne concentrations,  $^4He/^{20}Ne$  and  $^3He/^4He$   
410 with new data that cover part of the inter-eruptive periods between 2004 and 2018 (Vita  
411 et al., 2023).

412 Helium concentrations are in the range of  $9.2 \cdot 10^{-5}$ – $2.3 \cdot 10^{-3}$  cc/L at STP (Figure 6), with  
413 the highest values measured in COA, Limoneto, and Piscit a wells and the lowest in the  
414 Fulco well. Neon concentrations range between  $4.2 \cdot 10^{-5}$  and  $2.4 \cdot 10^{-4}$  cc/l at STP. The  
415  $^4He/^{20}Ne$  varies between 0.9 and 17.3 (Figures 6 and 7). In general, the  $R_c/R_a$  values do  
416 not show significant differences among the wells (Figure 7).

417 The  $^3He/^4He$  corrected for air contamination ( $R_c/R_a$ ) is in the range of 3.89–4.53  $R_a$   
418 (Figure 8). These ranges are in the same order of magnitude as those measured by  
419 Carapezza and Federico (2000), Inguaggiato and Rizzo (2004), Capasso et al. (2005), and  
420 Rizzo et al. (2009, 2015).

421

## 422 5 Discussion

423 ~~The geochemical investigation carried out on the thermal aquifer of Stromboli Island helped~~  
424 ~~improve our understanding of the processes affecting volcanic gases and the hydrological~~

425 system. This improved understanding has enhanced the potential for using fluid geochemistry for  
426 monitoring volcanic activity.

427 In the following discussion, we focus on:

428 ~~the processes controlling water chemistry, i.e. mixing between meteoric and marine water and~~  
429 ~~gas-water-rock interaction;~~

430 ~~the effects of gas-water interaction on the composition of volcanic gases;~~

431 ~~the potentiality of helium isotopes measured in the shallow aquifer for tracking the variable~~  
432 ~~input of early degassed primitive fluids.~~

433

### 434 5.1 Processes controlling water chemistry

435 Each site shows chemical variability due to different mixing between the meteoric  
436 recharge and seawater. Fresh groundwater usually lies upon brackish waters, and  
437 fluctuations of the water table can occur in coastal sites as an effect of tides (Singaraja et  
438 al., 2018) and the seasonal variability of the meteoric recharge (Liotta et al., 2006). As a  
439 consequence, even if the sampling of thermal water is always carried out using the same  
440 protocol (pumping flux, depth of the pump, duration of pumping before collecting  
441 samples, etc.), samples from the same sites show temporal variability of their salinity. In  
442 addition, such variability has different extents depending on the site features.

443 Among the elements that are enriched by the interaction with aquifer-hosting rocks  
444 (Capasso et al., 2005), K has the higher mobility since it does not precipitate as secondary  
445 phases, unlike Ca and Mg (e.g. calcite, Mg-calcite and gypsum), recognized in the  
446 hydrothermal alteration of the surface rocks (Finizola et al. 2002). Due to these  
447 characteristics, it offers the opportunity to evaluate the extent of water-rock interaction.  
448 In Figure 9, K is plotted versus Cl. All the samples exhibit a clear enrichment in K with  
449 respect to seawater. Samples from Fulco, Cusolito, Limoneto, Ossidiana, and Saibbo  
450 wells (with few exceptions probably due to direct seawater intrusion) fall around an  
451 alignment between Cusolito and FCDW. The alignment is indicative of a mixing process  
452 between a saline end-member (among the samples of Cusolito, EM3 in Figure 9) and the  
453 infiltrating water (FCDW and the poor saline samples from well Fulco, EM1 in Figure 9),  
454 being both enriched in K. This implies that also the shallow fresh waters interact with the  
455 hosting rocks and leach K. Conversely, samples from Zurro well show mixing between a  
456 saline end-member with high Cl content (one sample from Piscità well, EM2 in Figure 9)  
457 and a shallow end-member (represented by poor saline samples from well COA, EM4 in  
458 Figure 9). Samples from COA well show mixing between a saline end-member (EM3)  
459 enriched in K and a shallow end-member (EM4 in Figure 9). For both Zurro and COA  
460 samples, the shallow end-member (EM4) does not show a clear K-enrichment and  
461 probably reflects the rainfall composition. This suggests a fast infiltration of meteoric  
462 water and limited interaction with the hosting rocks.

463 The dissolution and hydration of magmatic CO<sub>2</sub> promote the chemical weathering of  
464 rocks. If the equilibrium is attained in the measured pH range, the carbonic acid  
465 dissociates as HCO<sub>3</sub><sup>-</sup>. Total alkalinity is a measure of CO<sub>2</sub>-water interaction and provides  
466 information about the paths through which CO<sub>2</sub> reaches the aquifer. In Figure 10 we show

467 that samples from Fulco, Cusolito, Limoneto, Ossidiana, and Saibbo define a negative  
 468 relationship between Cl and total alkalinity. Since ~~the~~ freshwater floats on ~~the~~ saline ~~one~~,  
 469 such a correlation implies that most of the CO<sub>2</sub> dissolved in water does not come from  
 470 depth but is carried by infiltrating waters. The ~~huge amount~~ of CO<sub>2</sub> degassing from s  
 471 (Inguaggiato et al., 2019 and reference therein) as well as the identification of a low  
 472 resistivity body in the summit area of the volcano (Revil et al., 2011 and references  
 473 therein), are consistent with the idea that meteoric waters infiltrating ~~in~~ the summit area  
 474 interact with CO<sub>2</sub> rising ~~from~~ fractures, favoring water-rock interaction and ~~the~~ increase  
 475 of the total alkalinity. A fraction of the total dissolved carbon reaches the basal aquifer as  
 476 dissolved CO<sub>2</sub>. At the Zurro site, the freshwater end-member exhibits low ~~values of~~ total  
 477 alkalinity, indicating ~~that~~ meteoric waters ~~infiltrate with limited interaction with~~ CO<sub>2</sub>.  
 478 Consequently, we observe a negative relationship between Cl and total alkalinity (Figure  
 479 10). At the COA site, samples display a large dispersion of ~~data~~ since the well is the most  
 480 elevated (70 m a.s.l.) and deepest. As a consequence, ~~it~~ intercepts several lithological  
 481 layers and receives different types of infiltrating waters (~~with different CO<sub>2</sub> contents~~).

482 The meteoric origin of fresh groundwater ~~was already~~ highlighted by Grassa et al. (2008)  
 483 using water stable isotopes. ~~An update of the dataset is shown~~ in Figure 3. All the  
 484 samples fall between the isotope composition of the Mediterranean seawater and the local  
 485 meteoric end-member defined by Liotta et al. (2006).

## 486 5.2 ~~The~~ gas/water interaction processes: dissolution-related gas fractionation

488 ~~The integrated dataset presented in this paper confirms the outcomes reported by Capasso~~  
 489 ~~et al. (2005) and Federico et al. (2008) on the chemical and C isotope composition of the~~  
 490 ~~gas dissolved in the Stromboli shallow aquifer.~~

491 ~~As shown in Figures 4 and 5,~~ the relative proportions of CO<sub>2</sub>, CH<sub>4</sub> and He vary in the  
 492 different sites and, in the same site, over time; moreover, the ~~highest~~ CO<sub>2</sub> contents also  
 493 have a C-isotope signature ~~close~~ to -1.5 permil, which is in the range of values measured  
 494 in the SC5 and Fossa fumaroles, in the summit area (Carapezza and Federico, 2000;  
 495 Finizola et al., 2003; Capasso et al., 2005; Rizzo et al., 2009), as well as in fluid  
 496 inclusions of olivine and clinopyroxene crystals separated from the San Bartolo  
 497 ultramafic cumulates (Gennaro et al., 2017). The CO<sub>2</sub>-poorer samples, namely Limoneto,  
 498 Piscità, and Cusolito, ~~instead,~~ have ~~more negative C-isotope composition~~ and ~~are~~  
 499 enriched in both He and CH<sub>4</sub> by more than two orders of magnitude compared to the air-  
 500 saturated water (ASW). Although the relationship shown in Figure 5, observed in other  
 501 volcanic and non-volcanic aquifers (Chiodini et al., 2000; Federico et al., 2002; Ohsawa  
 502 et al., 2002; Yamada et al., 2011), has generally been interpreted as ~~owing to the~~ mixing  
 503 between volcanic CO<sub>2</sub>-rich gases and soil CO<sub>2</sub>-~~poor~~ gases with ~~negative~~ isotope  
 504 composition, ~~typical of organic carbon,~~ other studies ~~interpreted~~ negative  $\delta^{13}\text{C}$  values as  
 505 due to fractionation of CO<sub>2</sub> during multistep dissolution ~~in water~~ (Simmons and  
 506 Christenson, 1994 and references therein). ~~According to Capasso et al. (2005) and~~  
 507 ~~Federico et al. (2008),~~ the dataset presented here suggests that some portions of the  
 508 aquifer are ~~reached~~ by a He-CH<sub>4</sub>-rich gas phase, derived from a volcanic gas modified

509 during the interaction with a multilevel hydrothermal aquifer, where the gases could  
510 separate and dissolve from one level to another. The multilevel aquifer is probably hosted  
511 by the alternating levels of lavas and pyroclastics in the subsoil of the Scari area, as  
512 suggested by Madonia et al. (2021). During gas-water interaction, different gas species  
513 would fractionate according to their solubility in water. The fraction process is described  
514 in Appendix 1.

515 The extent of Rayleigh's fractionation depends on the solubility of gases and the fraction  
516 of remaining gas (F) in equation 2 (Appendix 1), which could be considered as a proxy  
517 for the relative mass rates of the CO<sub>2</sub>-rich gas and the water with which it interacts. The  
518 larger the amount of gas interacting with a given volume of water in the time unit, the  
519 smaller the relative amount of gas removed upon dissolution, and the fraction of residual  
520 gas F (eq. 1) would be slightly lower than 1. In this case, the dissolved gas composition  
521 would not be significantly different from the initial one and would represent the deep  
522 volcano-hydrothermal gas. The CO<sub>2</sub>-richest samples from the Fulco well plot in  
523 correspondence with the highest values of F in Figure 4, which indicates that this well  
524 taps water levels entered by volcanic gases poorly modified by gas-water exchanges.  
525 Indeed, the area of Scari is considerably affected by the input of volcanic CO<sub>2</sub>  
526 (Inguaggiato et al., 2013; 2017) and some wells in this area, namely Fulco and Saibbo,  
527 have the highest dissolved CO<sub>2</sub> contents (290 and 180 cc/L at STP, respectively). On the  
528 contrary, in areas where the amount of gas interacting with the groundwater is lower, the  
529 extent of fractionation is larger, the fraction F of residual gas is significantly lower than  
530 1, and the residual gas would be significantly different from the initial gas. In the  
531 Stromboli aquifer, this modified gas composition characterizes the most saline samples,  
532 with Cl contents as high as about 550 mmol/L, namely those collected in the well Piscità  
533 well and some samples from the well Limoneto well. Due to the significant contribution  
534 of seawater, these wells are characterized by relatively higher pH values (average values  
535 from 6.7 to 7.1), and this plays a significant role in the fractionation process, due to the  
536 ability of basic aquifers to trap CO<sub>2</sub>.

537 In Figure 1, the groundwater He/CO<sub>2</sub> ratios are plotted versus the Cl contents, chosen as  
538 a proxy for seawater contribution.

539 The selected wells, namely COA, Limoneto, and Piscità, display variable Cl contents  
540 and, as commented in section 6.1, they result from the variable mixing between saline  
541 and meteoric-derived end members (namely from the mixing between the end-members  
542 EM1 and EM2 and EM4 and EM3). The highest He/CO<sub>2</sub> values, measured in the most  
543 saline well among them (Piscità), also correspond to the lowest CO<sub>2</sub> and alkalinity  
544 contents (Figure 10) and the highest He contents, which implies a mechanism of helium  
545 enrichment in the saline aquifer in response of the lower solubility in water of He  
546 compared to CO<sub>2</sub> (e.g., Capasso et al., 2005; Sander, 2015 and references therein). As  
547 observed in Figure 4, these samples show the highest He/CO<sub>2</sub> ratios and correspond to  
548 values of the fraction F of residual gas lower than 0.01. This well taps water levels where  
549 the input of volcanic gases is probably minor and/or the effect of CO<sub>2</sub> trapping in the  
550 aquifer at depth is locally enhanced by higher contamination of seawater.

551

## 552 5.3 Variations of water chemistry and dissolved gases

553 In Figure 12, the He/CO<sub>2</sub> and CH<sub>4</sub>/CO<sub>2</sub> ratios measured in water samples are plotted,  
 554 together with the theoretical curves derived from the processes of gas dissolution and  
 555 mixing. As in Figure 4, the theoretical curves are plotted by assuming three different  
 556 initial CH<sub>4</sub>/CO<sub>2</sub> values, from 5·10<sup>-5</sup> to 2·10<sup>-4</sup>, and He/CO<sub>2</sub> ratio of 2·10<sup>-5</sup>. ~~The process of~~  
 557 ~~gas dissolution is assumed to be a possible cause of variable gas concentrations in the~~  
 558 ~~aquifer because their effects are uneven in the whole basal aquifer.~~ Moreover, as  
 559 evidenced by water chemistry, ~~the mixing between water end members~~ of different  
 560 salinity, and different gas contents, can add further variability; in the different wells and  
 561 in a single well over time. ~~We underline that~~ salinity and gas contents are sometimes  
 562 related, as shown in Figure 11, which makes the processes of fractionation and mixing  
 563 seldom indistinguishable.

564 On these grounds, ~~by considering the end members identified in section 6.1 based on~~  
 565 ~~water chemistry, we tentatively~~ hypothesize various mixing trends which could account  
 566 for the variability observed among the wells and in a single well over time (Figures 12  
 567 and 13). The composition of air-saturated meteoric water (MW) and air-saturated  
 568 seawater (SW) are plotted for comparison.

569 By and large, as observed in Figure 13, the CO<sub>2</sub> contents decrease along with the increase  
 570 of Cl contents (Figure 13a), whereas CH<sub>4</sub> and He increase along with Cl contents.  
 571 Neither the air-saturated meteoric water (MW) nor the air-saturated seawater (SW) ~~do not~~  
 572 ~~represent a significant contribution~~ to the studied samples, which implies that a volcano-  
 573 hydrothermal gas phase, variably enriched in CO<sub>2</sub>, CH<sub>4</sub>, or He, prevails over  
 574 atmospheric gases, although the samples are meteoric or marine in origin. Samples from  
 575 the Zurro and Cusolito wells display a fairly narrow range of Cl contents (except for  
 576 some samples mixed with purely meteoric water), despite slightly variable CO<sub>2</sub>, CH<sub>4</sub> and  
 577 He contents. These two wells, both in the Scari area, are characterized by rather high  
 578 He/CO<sub>2</sub> values (Figure 12), which point ~~of~~ a fractionation upon the preferential  
 579 dissolution of CO<sub>2</sub>. Their salinity remains fairly homogeneous over time, so we could  
 580 hypothesize the variable contribution of gas enriched in He upon dissolution and gas less  
 581 fractionated and richer in CH<sub>4</sub> and CO<sub>2</sub>, whereas the mixing of different water types  
 582 should be negligible.

583 The mixing between end members of different salinity, and different CO<sub>2</sub>, He, and CH<sub>4</sub>  
 584 contents is demonstrated for wells Limoneto, COA, SAIBBO, and Fulco, as evident in  
 585 the graphs of Figure 13, and could be the origin of the variable composition detected in  
 586 these wells. End member EM1 is meteoric in origin, rich in CO<sub>2</sub>, and relatively poor in  
 587 CH<sub>4</sub> and He; the gas has a CH<sub>4</sub>/CO<sub>2</sub> ratio of around 2.5·10<sup>-5</sup> and a He/CO<sub>2</sub> ratio of  
 588 2.4·10<sup>-5</sup>, and is the less fractionated by dissolution in the shallow aquifer (curve 2 in  
 589 Figure 12). End member EM4, meteoric in origin like EM1, has a CH<sub>4</sub>-He-richer and  
 590 CO<sub>2</sub> poorer composition, probably deriving from the fractionation after dissolution (curve  
 591 2 in Figure 12); EM3, prevalently of marine origin, lies on the same Rayleigh curve as  
 592 EM4, at higher He and lower CO<sub>2</sub> contents, due to further fractionation. The mixing of  
 593 EM1 and EM4 end members (representing the poorest saline samples from Fulco and  
 594 COA) with EM3, already noted in Figure 9 to explain the composition of samples from

595 COA, is confirmed by the gas composition. The composition of some samples of COA  
596 ~~requires a~~ further contribution of CH<sub>4</sub>, as evident in Figure 13b. ~~According to what is~~  
597 ~~described so far,~~ the processes of fractionation upon dissolution and ~~the~~ mixing are  
598 ~~closely related,~~ and ~~probably~~ only when the water composition ~~does not vary it~~ would be  
599 possible to ~~ascertain~~ the variations exclusively related to ~~the~~ fractionation. While it is  
600 probable that ~~the~~ enrichment in He and, to some extent, CH<sub>4</sub> is related to gas  
601 fractionation during dissolution, apparently most effective in saline water bodies (see  
602 Figure 11), the temporal variations, at least in some cases, are ~~more~~ probably affected by  
603 the mixing between water bodies of different Cl content (and ~~different~~ gas composition),  
604 as in the case of Limoneto well (Figure 14). In other cases, the effects of mixing or  
605 fractionation upon dissolution are not clearly distinguishable and the scatter of the  
606 ~~measured~~ data compared to the ~~curves of~~ theoretical mixing ~~would confirm~~ the  
607 occurrence of both processes; ~~nevertheless, we could provide some suggestions about the~~  
608 ~~possible causes behind them.~~

609 The mixing between water bodies of different compositions is not surprising in a  
610 stratified aquifer, in a coastal area, where seawater-contaminated water levels lie below  
611 meteoric water levels and extend inland for tens or hundreds of meters. Additionally, the  
612 contribution of the magmatic-hydrothermal gas is uneven in the shallow aquifer and  
613 likely variable over time, thus increasing the spatial and temporal variability. In a single  
614 well, the dominance of one type of water or another can result from the variable meteoric  
615 input over time, from variations of the seawater level (Capasso et al., 2014), or  
616 modification of water circulation due to variations of crustal strain, as an effect of  
617 volcanic activity (Federico et al., 2017b and references therein). Additional information  
618 on the rainfall amount, the fluctuations of the sea level, and the water table elevation  
619 could ~~contribute to shedding~~ light on the effects of the different processes.

620 The fractionation of the volcanic gases upon dissolution ~~has to be~~ ascribed to the relative  
621 amount of gas and water in equilibrium in a given time unit and, ~~lastly,~~ to the mass rate of  
622 the volcanic gas compared to the water yield. The mass rate of gas entering the shallower  
623 water levels is supposed to be different in the various wells and, accordingly, the extent  
624 of Rayleigh's fractionation. In particular, the wells Fulco, SAIBBO, and COA tap water  
625 levels interact with a larger amount of volcanic gas, probably drained by the structural  
626 lineaments recognized by Finizola et al. (2002). The wells Piscità, Cusolito, and Zurro  
627 tap portions of the aquifer ~~deeply~~ contaminated by hot seawater (modified by water-rock  
628 exchanges, as testified by the enrichment in K, Figure 9), interacting with lower amounts  
629 of volcanic gases, ~~deeply~~ modified by the fractionation due to dissolution.

630

#### 631 5.4 Chemistry of noble gases

632 As already highlighted and modeled in Section 6.2, the concentration (in cc/L at STP) of  
633 <sup>4</sup>He dissolved in thermal waters from different wells differs mostly in response to its  
634 preferential partitioning into the vapor phase compared to CO<sub>2</sub>. Instead, <sup>20</sup>Ne  
635 concentration ~~does~~ not show the same ~~differences~~ among the wells, although <sup>20</sup>Ne and  
636 <sup>4</sup>He solubility in water is comparable (Sander, 2015). In detail, the concentration of <sup>20</sup>Ne



637 varies in a range of values that includes the theoretical value in air-saturated water and is  
638 comparable among the different wells, irrespective of the extent of the fractionation due  
639 to gas-water interaction. This indicates that the mixing between magmatic and  
640 atmospheric fluids mostly modulates the variability of  $^{20}\text{Ne}$  concentration, further  
641 supporting the idea that hydrothermal vapor mixes with the shallower meteoric aquifer,  
642 variably contaminated by seawater (Capasso et al., 2005; Grassa et al., 2008 and this  
643 work). Consequently, the atmospheric neon completely masks that of magmatic origin,  
644 which we expect to have a concentration of 2-3 orders of magnitude lower. Following  
645 this evidence, we argue that  $^{20}\text{Ne}$  cannot be useful to evaluate the extent of gas-water  
646 interaction in the different wells and, more importantly, that the variability of  $^4\text{He}/^{20}\text{Ne}$  is  
647 mostly modulated by the variability of  $^4\text{He}$  concentration, as can be visualized in Figure  
648 6. Indeed, Limoneto and Piscità wells that show the highest enrichment in  $^4\text{He}$  also  
649 display the highest  $^4\text{He}/^{20}\text{Ne}$  values (Figure 6). This could theoretically affect the  
650 correction of atmospheric contamination, which is based on the  $^4\text{He}/^{20}\text{Ne}$  ratios.  
651 Nevertheless, considering that  $^4\text{He}/^{20}\text{Ne}$  values are generally at least one order of  
652 magnitude higher than in ASW ( $^4\text{He}/^{20}\text{Ne} = 0.285$ ) even in those wells less modified by  
653 the fractionation due to gas-water interaction, we point out that the  $R_c/R_a$  corrected values  
654 generally differ from measured  $R/R_a$  values of less than  $0.2 R_a$ , leading us to consider the  
655 correction we applied as reliable. Some exceptions regard a few samples of the Cusolito,  
656 Fulco, and Zurro wells sampled during 2004-2008 that showed among the lowest  $^4\text{He}$   
657 content and  $^4\text{He}/^{20}\text{Ne}$  next to or below 1, which probably led to an uncertainty in the  
658 correction of  $^3\text{He}/^4\text{He}$  and an underestimation of  $R_c/R_a$  values.

#### 659 5.4.1 Statistical evaluation of $^3\text{He}/^4\text{He}$ ratios in the thermal aquifer

660 The regular monitoring of  $^3\text{He}/^4\text{He}$  at Stromboli allows a statistical evaluation of  
661 the dataset. Because  $^3\text{He}/^4\text{He}$  ratios are not fractionated by gas-water interaction in  
662 the hydrothermal aquifer, they preserve their original signature and are thus used  
663 within the INGV-Palermo monitoring protocol. ~~For these reasons, we focus our~~  
664 ~~statistical evaluation on this tracer.~~ We already noted that there is no difference in  
665 the  $^3\text{He}/^4\text{He}$  signature among the various wells, therefore our discussion concerns  
666 the whole dataset. Considering the discrete sampling of the seven thermal wells, a  
667 total of 511 measurements of  $^3\text{He}/^4\text{He}$  were carried out during 2004-2018. The He  
668 isotopic ratios vary between  $3.74$  and  $4.56 R_a$  with a mean  $\pm$  standard deviation of  
669  $4.24 \pm 0.13 R_a$ . In terms of frequency, 63 measurements fall below  $4.1 R_a$ ,  
670 equivalent to 12% of the dataset, 398 between  $4.1$  and  $4.4 R_a$ , equivalent to 78%,  
671 and 50 above  $4.4 R_a$ , equivalent to 10% (Figure 15). Considering that i) magma  
672 replenishments by poorly degassed melts are characterized by increasing  $^3\text{He}/^4\text{He}$   
673 values (Capasso et al., 2005; Rizzo et al., 2009, 2015; Martelli et al., 2014), ii) the  
674 maximum values measured in phenocrysts of LP magma are about  $4.6 R_a$   
675 (Martelli et al., 2014), and iii) the highest  $^3\text{He}/^4\text{He}$  values ( $4.50$ - $4.56 R_a$ ) were  
676 always measured during eruptive phases characterized by weeks to months of lava  
677 effusion (Rizzo et al., 2009, 2015; Martelli et al., 2014), we conclude that  $^3\text{He}/^4\text{He}$   
678 values exceeding  $4.4 R_a$  represent phases of dominant degassing of the LP  
679 magma, able to potentially feed high magmatic activity.

#### 680 5.4.2 Variations of $^3\text{He}/^4\text{He}$ ratios in relation to volcanic activity

681 ~~We now evaluate the temporal variations of  $^3\text{He}/^4\text{He}$  ratios ( $R_c/R_a$  units) in~~  
 682 ~~relation to the volcanic activity during 2004-2018 (Figure 8).~~ To the best of our  
 683 knowledge, this is the first time that a data set of fourteen years of regular  
 684 measurements of  $^3\text{He}/^4\text{He}$  is presented and discussed in a single volcanic system,  
 685 offering a unique opportunity to better comprehend the short- and long-term  
 686 evolution of the magmatic activity of Stromboli.

687 As highlighted in the previous studies by Capasso et al. (2005) and Rizzo et al.  
 688 (2008, 2009, 2015), the sampled wells have a comparable range of  $R_c/R_a$  values  
 689 (3.7-4.5  $R_a$ ) and temporal variations of  $^3\text{He}/^4\text{He}$  that occurred almost  
 690 simultaneously (Figure 8). This is confirmed for the periods of monitoring 2004-  
 691 2005, 2008-2009, and 2015-2018 that are presented in this study for the first time,  
 692 supporting the idea that the magmatic fluids dissolving in the hydrothermal  
 693 aquifer have a common source. However, an important difference in  $R_c/R_a$  values  
 694 can be observed between 2002-2007 and 2008-2018: during 2002-2007, the range  
 695 of  $^3\text{He}/^4\text{He}$  varied between 3.7 and 4.5  $R_a$  with a mean  $\pm$  standard deviation of  
 696  $4.19 \pm 0.13 R_a$ , whereas during 2008-2018 it moves from 4.2 to 4.6  $R_a$  with a  
 697 mean of  $4.34 \pm 0.08 R_a$  (Figure 8). The entire period of monitoring (2002-2018)  
 698 has a mean  $^3\text{He}/^4\text{He}$  of  $4.24 \pm 0.13 R_a$ . In detail, since 2008 onwards we have not  
 699 measured  $^3\text{He}/^4\text{He}$  lower than 4.2  $R_a$  (except one sample from COA), in contrast  
 700 to what was observed from 2001 to 2007, and there is a reduced variability in the  
 701  $^3\text{He}/^4\text{He}$  ratios of each well (Figure 8). However, the highest  $R_c/R_a$  values never  
 702 exceeded 4.6  $R_a$  during 2002-2018. We suggest that the differences between the  
 703 two periods could ~~depend on~~ a modification of the degassing path and the  
 704 magmatic activity of the volcano (Calvari et al., 2014), which could have ~~been~~  
 705 favored ~~by~~ an enhanced contribution of the  $^3\text{He}$ -rich LP melt.

706 During 2004-2014,  $R_c/R_a$  values  $\geq 4.4$  were measured during and/or in the  
 707 proximity of the effusive eruptions of 2007, and 2014, and in periods of an  
 708 increased occurrence of major explosions (Bevilacqua et al., 2020), as in 2017-  
 709 2018. These values approached the maximum  $^3\text{He}/^4\text{He}$  (i.e., 4.6  $R_a$ ) measured by  
 710 Martelli et al. (2014) in fluid inclusions hosted in olivine and clinopyroxene from  
 711 LP volatile-rich pumices. These high  $R_c/R_a$  values were interpreted as due to the  
 712 enhanced contribution of gas from a new batch of LP magma which prevails over  
 713 the degassing of the residing HP magma. Therefore, the temporal variations of the  
 714  $^3\text{He}/^4\text{He}$  ratio can be explained as a mixing of volatiles persistently emitted from  
 715 LP magma ( $^3\text{He}/^4\text{He}$  ratio  $\geq 4.6 R_a$ ) with those degassed from batches of magma  
 716 resident in the shallow portions of the plumbing system up to the HP reservoir (~  
 717 2 km below the sea level; e.g., Métrich et al., 2010, 2021 and references therein).  
 718 This model was already proposed to explain the variability in the composition of  
 719 plume gases emitted from the craters (Aiuppa et al., 2010). In addition, we recall  
 720 that the continuous refilling of the shallow magma body by deep volatile-rich  
 721 magmas, together with the continuous magma emission, ~~determines~~ the steady  
 722 state of the Stromboli plumbing system (e.g., Landi et al., 2009; Métrich et al.,  
 723 2010). The shallow batches of magma would reasonably have a  $^3\text{He}/^4\text{He}$  signature  
 724 (not yet constrained) lower than LP magma. This signature would result from the

725 addition of radiogenic  $^4\text{He}$ , produced from U and Th contained in differentiated  
 726 rocks in contact with the magma, to the residual helium dissolved at low  
 727 concentrations in the extensively degassed melts. We cannot exclude that part of  
 728 this shallow contamination occurs within the hydrothermal system. The temporal  
 729 variations as well as the absolute values of  $^3\text{He}/^4\text{He}$  measured in the fluids  
 730 resulting from the hypothesized mixing and last dissolving in the hydrothermal  
 731 aquifer of Stromboli, would largely be ~~mostly~~ regulated by the mass rate of  
 732 volatiles degassed from the LP magma, which depends on the magma dynamics at  
 733 depth. Further studies aimed at better constraining the  $^3\text{He}/^4\text{He}$  signature of  
 734 magmas residing in the shallowest portions of the plumbing system and feeding  
 735 ordinary activity of Stromboli (i.e., HP magma), as well as the path and depth of  
 736 helium degassing from the mantle, would enable quantitative refinement of this  
 737 interpretative model.

738 ~~Having updated the period of monitoring to June 2018, we can better detail the~~  
 739 ~~evolution after the 2014 eruption (Figure 8). The data series presented by Rizzo et~~  
 740 ~~al. (2015) stopped on 24 November 2014, when  $^3\text{He}/^4\text{He}$  values were still high~~  
 741 ~~(Figure 7). After then and~~ until April 2016, the  $R_c/R_a$  values remained high ( $\sim 4.4$   
 742  $R_a$ ) while the resumption of Strombolian activity was ongoing. After April 2016,  
 743 the  $^3\text{He}/^4\text{He}$  decreased to average values, which represent almost 80% of the  
 744 dataset (Figure 17). Since September 2017, a new increase of  $^3\text{He}/^4\text{He}$  ratios was  
 745 observed with values as high as  $4.5 R_a$  at the end of November 2017 (Figure 8).  
 746 After this peak,  $R_c/R_a$  values varied around medium-to-medium-high values until  
 747 June 2018. We highlight that during 2017-2018, the activity at Stromboli was  
 748 characterized by an increase in the rate of occurrence of Strombolian explosions  
 749 as well as by the occurrence of several explosions of major intensity and lava  
 750 overflows (Giudicepietro et al., 2019). During the same period, Inguaggiato et al.  
 751 (2019) reported a progressive increase of  $\text{CO}_2$  degassing from the soil in the  
 752 summit area, further supporting the idea that the level of activity of Stromboli was  
 753 increasing again in that period.

754 We argue that the increases in the  $^3\text{He}/^4\text{He}$  ratios recorded in 2017-2018 can be  
 755 explained as a variable replenishment of the deep ( $>7$ -10 km) portions of the  
 756 plumbing system by the LP magma. It is reasonable to suppose that this  
 757 replenishment progressively pressurized the main zone of storage of LP magma  
 758 up to critical conditions.

## 759 5.5 Input of volcanic fluids in the shallow aquifer: an interpretative model

760 ~~As discussed so far, the interaction of volcanic hydrothermal fluids with the shallow~~  
 761 ~~basal aquifer in Stromboli produces a complex scenario. In the area of Seari, magmatic~~  
 762 ~~fluids, emitted throughout the shallow conduit system, permeate along discontinuities,~~  
 763 ~~condense in shallower and colder portions of the volcanic edifice, and undergo chemical~~  
 764 ~~and physical modifications, in response to non-magmatic temperature and redox~~  
 765 ~~conditions. The development of hydrothermal systems is hypothesized or indirectly~~  
 766 ~~observed in many volcanic systems worldwide and, specifically, in volcanic islands~~

~~767 (Fournier, 1999; Hedenquist and Lowenstern, 1994; Valsami-Jones et al., 2005; Aizawa  
768 et al., 2009; Villasante-Marcos et al., 2014).~~

769 ~~The investigations performed by Revil et al. (2011) gave evidence of a~~ conductive zone  
770 ~~in the central portion of the volcanic edifice, interpreted as the main hydrothermal~~  
771 ~~system, and an advective hydrothermal circulation downward E and NE, in the area of~~  
772 ~~Scari. The boundary between hydrothermal water and groundwater was estimated at~~  
773 ~~about 100+/- 60 m asl, while the intrusion of the seawater was assumed to be as low as -3~~  
774 ~~km in depth (figure 16).~~

775 ~~According to Revil et al. (2011), the main hydrothermal system is localized in the central~~  
776 ~~part of the volcanic edifice up to the area of Pizzo, has a deep root, and releases the~~  
777 ~~hydrothermal fluids circulating in the area of Stromboli village. In the summit area of~~  
778 ~~Pizzo, then, we should expect the strongest magmatic signature of  $^3\text{He}/^4\text{He}$ . Instead, the~~  
779 ~~highest ratios are measured in the thermal water wells of Stromboli village, while~~  
780 ~~fumarole gases located at Pizzo Sopra La Fossa (SC5) display  $^3\text{He}/^4\text{He}$  values about 1~~  
781 ~~unit Ra lower than those measured in the basal aquifer (Carapezza and Federico, 2000;~~  
782 ~~Capasso et al., 2005, Rizzo et al., 2009). Therefore, we argue that magmatic fluids~~  
783 ~~degassed from melts at depth, first dissolve in a hydrothermal system localized below the~~  
784 ~~sea level and close to the main conduits, and then ascend to the summit area, where the~~  
785 ~~leaching of old and differentiated rocks provides radiogenic  $^4\text{He}$ , deriving from the decay~~  
786 ~~of U and Th, and thus decreases the  $^3\text{He}/^4\text{He}$  of Pizzo Sopra La Fossa fumaroles.~~

787 There is geochemical evidence that the unconfined meteoric aquifer is variably  
788 contaminated by seawater, which infiltrates deep inside the volcanic edifice and is  
789 overlaid by the meteoric water. The saline water tapped by some of the wells (namely  
790 Piscità, Zurro, and Cusolito), albeit marine origin, is deeply modified by the input of  
791 thermal fluids and by water-rock interaction. This confirms that the hydrothermal  
792 circulation is certainly rooted within the volcanic edifice below the seawater level.

793 The composition of the dissolved gas marks some peculiarities among the different water  
794 levels tapped by the studied wells. As observed in the Piscità well, the  $\text{CO}_2$ -poor and  
795  $\text{CH}_4$ -He-rich composition, together with a temperature higher than  $30^\circ\text{C}$ , would be  
796 compatible with the interaction with hot volcanic fluids, whose composition is modified  
797 by the removal of  $\text{CO}_2$  in deeper and, probably, saline water levels, promoted by a  
798 relatively low gas flux, according to a mechanism of Rayleigh's fractionation, as  
799 described in section 6.2. The contribution of  $\text{CH}_4$  observed in all the monitored wells is  
800 probably derived from the boiling of a typical hydrothermal system. In some cases,  
801 (either in seawater-derived samples such as Zurro and Cusolito or meteoric-derived  
802 samples, such as COA and Limone), the hydrothermal gas undergoes further  
803 fractionation during its traveling toward the shallower levels of the aquifer. The  
804 monitored wells show variations in water chemistry, due to variable mixing of the  
805 meteoric/saline water, paralleled by different  $\text{CO}_2$ -He and  $\text{CH}_4$  contents. The  
806 compositional variability of the groundwater leads to difficulty in ascertaining the  
807 variable contribution over time of gas of different origins (hydrothermal or prevalently  
808 magmatic), possibly modified by dissolution. Probably, variations in gas composition not  
809 paralleled by variations in water composition could be ascribed to a variable input of

810 magmatic or hydrothermal gases, to variation in their composition, and/or to Rayleigh's  
811 type fractionation, whereas variations in water chemistry point to the mixing between  
812 waters, different in both chemistry and gas contents.

## 813 **6 Conclusions**

814 The long-term monitoring of the Stromboli basal aquifer allowed the development of a  
815 comprehensive framework of the interactions among magmatic-hydrothermal fluids and shallow  
816 water. The complexity related to the presence of meteoric water, extensively contaminated by  
817 seawater and modified by water-rock exchanges, the reactivity of ~~(most)~~ the volcanic gas  
818 species, and their different solubility in water, requires some caution when interpreting ~~of~~ the  
819 observed variations in both water and gas chemistry. The monitored wells tap water levels that  
820 are variably contaminated by seawater and CH<sub>4</sub>-rich hydrothermal fluids and are characterized  
821 by different CO<sub>2</sub> and He contents. Besides the mixing of different water types, the gas  
822 composition ~~is expected to vary~~ as an effect of i) the different solubility in water of gas species  
823 and the variable input of gas over time, which primarily controls the extent of the gas  
824 fractionation in water; ii) different contributions of magmatic and hydrothermal gases. ~~We~~  
825 ~~suggest that~~ rainfall amounts, fluctuations of the seawater level and the water table head in the  
826 wells must be routinely monitored, to determine the hydrological causes of the variations in  
827 water chemistry.

828 The long-term monitoring of helium isotopes in thermal waters has demonstrated that i) thermal  
829 waters have dissolved helium with a magmatic signature that varies in response to medium- to  
830 long-term changes in magmatic dynamics at depth and represents a safe method for monitoring  
831 the activity of the volcano; ii) low to ordinary activity is generally characterized by <sup>3</sup>He/<sup>4</sup>He  
832 values below 4.4 Ra, whereas <sup>3</sup>He/<sup>4</sup>He values greater than 4.4 Ra probably derive from a higher  
833 contribution of gas emitted from the LP magma, which may prelude an increase in the eruptive  
834 activity.

## 835 **Acknowledgments**

836 The authors wish to thank their colleagues at the Istituto Nazionale di Geofisica e Vulcanologia  
837 of Palermo for their contribution in collecting samples and analyzing data. All the chemical and  
838 isotopic data were produced in the Geochemical Laboratories of INGV Palermo. This research  
839 was funded by the INGV-DPCN (Italian National Institute of Geophysics and Volcanology-  
840 Italian National Department for Civil Protection) volcanic surveillance program of Stromboli  
841 volcano. ObFu 0304.010.

## 843 **Data Availability Statement**

844  
845 All the data produced in this work are publicly available in the Earthchem data repository (Vita  
846 et al., 2023).

847

848

849 **References**

850 Aiuppa, A., Bertagnini, A., Métrich, N., Moretti, R., Di Muro, A., Liuzzo, M., Tamburello, G.,  
851 (2010), A model of degassing for Stromboli volcano, 10.1016/j.epsl.2010.03.040, *Earth Planet.*  
852 *Sci. Lett.* 295, 95-204.

853 Aizawa, K., Ogawa, Y., & Ishido, T. (2009), Groundwater flow and hydrothermal systems  
854 within volcanic edifices: Delineation by electric self-potential and magnetotellurics, *Journal of*  
855 *Geophysical Research: Solid Earth*, 114(B1). <https://doi.org/10.1029/2008JB005910>.

856 Albarède F. (1995), Introduction to geochemical modeling. Cambridge University Press,  
857 Cambridge

858 Andronico, D., Del Bello, E., D’Oriano, C., Landi, P., Pardini, F., Scarlato, P., ... & Valentini, F.  
859 (2021), Uncovering the eruptive patterns of the 2019 double paroxysm eruption crisis of  
860 Stromboli volcano, *Nature Communications*, 12(1), 4213.

861 Antoine, R., Baratoux, D., Rabinowicz, M., Fontaine, F., Bachelery, P., Staudacher, T., Saracco,  
862 G., Finizola, A., 2009, Thermal infrared image analysis of a quiescent cone on Piton de la  
863 Fournaise volcano: evidence of convective air flow within an unconsolidated soil, *J. Volcanol.*  
864 *Geotherm. Res.* 183, 228–244.

865 Bertagnini, A., Métrich, N., Francalanci, L., Landi, P., Tommasini, S., Conticelli, S. (2008).  
866 Volcanology and magma geochemistry of the present-day activity: constraints on the feeding  
867 system. In: Calvari, S., Inguaggiato, S., Puglisi, G., Ripepe, M., Rosi, M. (Eds.), Learning from  
868 Stromboli. Geophysical Monograph 182. American Geophysical Union, pp. 19–38.

869 Bevilacqua, A., Bertagnini, A., Pompilio, M., Landi, P., Del Carlo, P., Di Roberto, A., ... & Neri,  
870 A. (2020), Major explosions and paroxysms at Stromboli (Italy): A new historical catalog and  
871 temporal models of occurrence with uncertainty quantification, *Scientific reports*, *10*(1), 17357.

872 Caliro, S., Caracausi, A., Chiodini, G., Ditta, M., Italiano, F., Longo, M., Minopoli, C., Nuccio,  
873 P.M., Paonita, A., Rizzo, A. (2004), Evidence of a recent input of magmatic gases into the  
874 quiescent volcanic edifice of Panarea, Aeolian Islands, Italy, *Geophys. Res. Lett.* *31*, L07619.

875 Caliro S., Chiodini G., Moretti R., Avino R., Granieri D., Russo M. and Fiebig J. (2007), The  
876 origin of the fumaroles of La Solfatara (Campi Flegrei, South Italy), *Geochim. Cosmochim. Acta*  
877 *71*, 3040–3055. <http://dx.doi.org/10.1016/j.gca.2007.04.007>.

878 Calvari, S., et al. (2014), Major eruptive style changes induced by structural modifications of a  
879 shallow conduit system: The 2007–2012 Stromboli case, *Bull. Volcanol.*, doi:10.1007/s00445-  
880 014-0841-7.

881 Capasso, G. and Inguaggiato, S. (1998), A simple method for the determination of dissolved  
882 gases in natural waters: An application to thermal waters from Vulcano island, *Applied*  
883 *Geochem.*, *13*, 631-642.

884 Capasso, G., Favara, R., Francofonte, S., & Inguaggiato, S. (1999), Chemical and isotopic  
885 variations in fumarolic discharge and thermal waters at Vulcano Island (Aeolian Islands, Italy)  
886 during 1996: evidence of resumed volcanic activity, *Journal of volcanology and geothermal*  
887 *research*, *88*(3), 167-175.

888 Capasso G., Carapezza M. L., Federico C., Inguaggiato S. and Rizzo A. (2005), Geochemical  
889 monitoring of the 2002–2003 eruption at Stromboli volcano (Italy): precursory changes in the  
890 carbon and helium isotopic composition of fumarole gases and thermal waters, *Bull. Volcanol.*  
891 *68*, 118–134.

- 892 Capasso, G., Federico, C., Madonia, P., & Paonita, A. (2014), Response of the shallow aquifer of  
893 the volcano-hydrothermal system during the recent crises at Vulcano Island (Aeolian  
894 Archipelago, Italy), . *Volcanol. Geotherm. Res.*, 273, 70-80.
- 895 Carapezza M. L. and Federico C. (2000), The contribution of fluid geochemistry to the volcano  
896 monitoring of Stromboli, *J. Volcanol. Geotherm. Res.* 95, 227–245.
- 897 Carapezza, M. L., Inguaggiato, S., Brusca, L., and Longo, M. (2004), Geochemical precursors of  
898 the activity of an open-conduit volcano: The Stromboli 2002-2003 eruptive events, *Geoph. Res.*  
899 *Letters*, 31, L07620.
- 900 Carapezza, M.L., Ricci, T., Ranaldi, M. & Tarchini, L. (2009), Active degassing structures of  
901 Stromboli and variations in diffuse CO<sub>2</sub> output related to the volcanic activity, *J. Volc.*  
902 *Geotherm. Res.*, 182, 231–245.
- 903 Chiodini G., Cioni R., Marini L., and Panichi C. (1995), Origin of the fumarolic fluids of  
904 Vulcano Island, Italy, and implications for volcanic surveillance, *Bull. Volcanol.* 57, 99–110.
- 905 Chiodini, G., Frondini, F., Cardellini, C., Parello, F., & Peruzzi, L. (2000), Rate of diffuse carbon  
906 dioxide Earth degassing estimated from carbon balance of regional aquifers: The case of central  
907 Apennine, Italy, *Journal of Geophysical Research: Solid Earth*, 105(B4), 8423-8434.
- 908 Chiodini, G., Marini, L., and Russo, M. (2001), Geochemical evidence for the existence of high  
909 temperature brines at Vesuvio volcano, Italy, *Geochem. Cosm. Acta* 65, 2129–2147.
- 910 Chiodini, G., Granieri, D., Avino, R., Caliro, S., Costa, A., Werner, C. (2005), Carbon dioxide  
911 diffuse degassing and estimation of heat release from volcanic and hydrothermal systems, *J.*  
912 *Geophys. Res.* 110, B08204. <http://dx.doi.org/10.1029/2004JB003542>.



913 Chiodini, G., Paonita, A., Aiuppa, A. et al. 2016, Magmas near the critical degassing pressure  
914 drive volcanic unrest towards a critical state. *Nat Commun* 7, 13712.  
915 <https://doi.org/10.1038/ncomms13712>

916 Deines P, Langmuir D, Harmon RS (1974) Stable carbon isotope ratios and the existence of a gas  
917 phase in the evolution of carbonate groundwaters. *Geochim Cosmochim Acta* 38:1147–1164

918 Ellam, R.M., Hawkesworth, C.J., Menzies, M.A., Rogers, N.W., 1989. The volcanism of  
919 southern Italy: role of subduction and relationship between potassic and sodic alkaline  
920 magmatism. *J. Geophys. Res.* 94, 4589–4601.

921 Federico, C., Aiuppa, A., Allard, P., Bellomo, S., Jean-Baptiste, P., Parello, F., & Valenza, M.  
922 (2002). Magma-derived gas influx and water-rock interactions in the volcanic aquifer of Mt.  
923 Vesuvius, Italy. *Geochimica et Cosmochimica Acta*, 66(6), 963-981.

924 Federico, C., Brusca, L., Carapezza, M. L., Cigolini, C., Inguaggiato, S., Rizzo, A., & Rouwet,  
925 D. (2008). Geochemical prediction of the 2002-2003 Stromboli eruption from variations in CO<sub>2</sub>  
926 and Rn emissions and in helium and carbon isotopes. In: *Learning from Stromboli and its 2002-*  
927 *03 eruptive crisis*. AGU, 2008 Washington DC American Geophysical Union Geophysical  
928 *Monograph Series*, 182, 117-128.

929 Federico, C., Capasso, G., Paonita, A., Favara, R. (2010) Effects of steam-heating processes on a  
930 stratified volcanic aquifer: Stable isotopes and dissolved gases in thermal waters of Vulcano  
931 Island (Aeolian archipelago). *Journal of Volcanology and Geothermal Research*, 192, 178-190.

932 Federico C., Inguaggiato, S., Chacón, Z., Londoño, JM., Gil, E., Alzate, D. (2017a) Vapour  
933 discharges on Nevado del Ruiz during the recent activity: Clues on the composition of the deep  
934 hydrothermal system and its effects on thermal springs - *Journal of Volcanology and Geothermal*  
935 *Research*, 2017; <https://doi.org/10.1016/j.jvolgeores.2017.04.007>

- 936 Federico, C., Longo, M., D'Alessandro, W., Bellomo, S., Bonfanti, P., & Brusca, L. (2017b).  
937 Hydrological versus volcanic processes affecting fluid circulation at Mt. Etna: inferences from  
938 10 years of observations at the volcanic aquifer. *Chemical Geology*, 452, 71-84.
- 939 Finizola A., Sortino F., Lénat J.-F. and Valenza M. (2002) Fluid circulation at Stromboli volcano  
940 (Aeolian Islands, Italy) from self-potential and CO<sub>2</sub> surveys. *J. Volcanol. Geotherm. Res.* 116,  
941 1–18.
- 942 Finizola A, Sortino F (2003) Preliminary model of fluid circulation at Stromboli volcano inferred  
943 by water and gas geochemistry. ICGG7-A-00108, 22-26 September 2003 Freiberg, Germany
- 944 Finizola, A., Sortino, F., Lénat, J. F., Aubert, M., Ripepe, M., & Valenza, M. (2003). The  
945 summit hydrothermal system of Stromboli. New insights from self-potential, temperature, CO<sub>2</sub>  
946 and fumarolic fluid measurements, with structural and monitoring implications. *Bulletin of*  
947 *Volcanology*, 65, 486-504.
- 948 Finizola, A., Revil, A., Rizzo, E., Piscitelli, S., Ricci, T., Morin, J., Angeletti, B., Mocochain, L.,  
949 Sortino, F., 2006. Hydrogeological insights at Stromboli volcano (Italy) from geoelectrical,  
950 temperature, and CO<sub>2</sub> soil degassing investigations. *Geophys. Res. Lett.* 33, L17304.  
951 doi:10.1029/2006GL026842
- 952 Finizola, A., Aubert, M., Revil, A., Schutze, C., Sortino, F. (2009). Importance of structural  
953 history in the summit area of Stromboli during the 2002–2003 eruptive crisis inferred from  
954 temperature, soil CO<sub>2</sub>, self-potential, and electrical resistivity tomography. *Journal of*  
955 *Volcanology and Geothermal Research*, 183, 213-227.
- 956 Finizola, A., Ricci, T., Deiana, R., Cabusson, S. B., Rossi, M., Praticelli, N., ... & Lelli, M.  
957 (2010). Adventive hydrothermal circulation on Stromboli volcano (Aeolian Islands, Italy)

958 revealed by geophysical and geochemical approaches: implications for general fluid flow models  
959 on volcanoes. *Journal of Volcanology and Geothermal Research*, 196(1-2), 111-119.

960 Fournier, R. O. (1999), Hydrothermal processes related to movement of fluid from plastic into  
961 brittle rock in the magmatic-epithermal environment, *Econ. Geol.*, 94, 1193–1211.

962 Francalanci, L., Manetti, P., Peccerillo, A., Keller, J., 1993. Magmatological evolution of the  
963 Stromboli volcano (Aeolian Arc, Italy): inferences from major and trace element and Sr-isotopic  
964 composition of lavas and pyroclastic rocks. *Acta Vulcanol.* 3, 127–151.

965 Francalanci, L., Tommasini, S., Conticelli, S., 2004. The volcanic activity of Stromboli in the  
966 1906–1998 period: mineralogical, geochemical and isotope data relevant to the understanding of  
967 Strombolian activity. *J. Volcanol. Geotherm. Res.* 131, 179–211.

968 Francalanci, L., Avanzinelli, R., Tommasini, S., Heuman, A., 2007. A west–east geochemical and  
969 isotopic traverse along the volcanism of the Aeolian Island arc, southern Tyrrhenian Sea, Italy:  
970 inferences on mantle source processes. In: Beccaluva, L., Bianchini, G., Wilson, M. (Eds.),  
971 *Cenozoic Volcanism in the Mediterranean Area*. Geological Society of America, Denver, U.S.A.,  
972 pp. 235–263.

973 Gasparini, C., G. Iannaccone, P. Scandone, and R. Scarpa (1982), Seismotectonics of the  
974 Calabrian Arc, *Tectonophysics*, 84, 267–286.

975 Gat, J. R., and I. Carmi (1970), Evolution of the isotopic composition of atmospheric waters in  
976 the Mediterranean Sea area, *J. Geophys. Res.*, 75, 3039–3048, doi:10.1029/JC075i015p03039.

977 Gat J. R., Shemesh A., Tziperman E., Hecht A., Georgopoulos D. and Basturk O. (1996) The  
978 stable isotope composition of waters of the eastern Mediterranean Sea. *J. Geophys. Res. Ocean.*  
979 101, 6441–6451.

- 980 Gennaro, M. E., F. Grassa, M. Martelli, A. Renzulli, and A. L. Rizzo (2017). Carbon isotope  
981 composition of CO<sub>2</sub>-rich inclusions in cumulate-forming mantle minerals from Stromboli  
982 volcano (Italy). *J. Volcanol. Geotherm. Res.*, 1–9,  
983 <http://dx.doi.org/10.1016/j.jvolgeores.2017.04.001>
- 984 Giggenbach, W.F. (1975). A simple method for the collection and analysis of volcanic gas  
985 samples, *Bull. Volcanol.* 39, 132–145.
- 986 Giudicepietro, F., Calvari, S., Alparone, S., Bianco, F., Bonaccorso, A., Bruno, V., Caputo, T.,  
987 Cristaldi, A., D’Auria, L., De Cesare, W., Di Lieto, B., Esposito, A.M., Gambino, S.,  
988 Inguaggiato, S., Macedonio, G., Martini, M., Mattia, M., Orazi, M., Paonita, A., Peluso, R.,  
989 Privitera, E., Romano, P., Scarpato, G., Tramelli, A., Vita, F. (2019). Integration of Ground-  
990 Based Remote-Sensing and In Situ Multidisciplinary Monitoring Data to Analyze the Eruptive  
991 Activity of Stromboli Volcano in 2017–2018. *Remote Sens.* 2019, 11, 1813;  
992 [doi:10.3390/rs11151813](https://doi.org/10.3390/rs11151813)
- 993 Grassa, F., Inguaggiato, S., Liotta, M. (2008), Fluids geochemistry of Stromboli. In “The  
994 Stromboli Volcano – An Integrated study of the 2002-2003 Eruption” AGU Geophysical  
995 monograph” 182, 49-63.
- 996 Hedenquist, J. W., and J. B. Lowenstern (1994), The role of magmas in the formation of  
997 hydrothermal ore deposits, *Nature*, 370, 519–527, [doi:10.1038/370519a0](https://doi.org/10.1038/370519a0).
- 998 Inguaggiato, S., Pecoraino, G., and D’Amore, F., 2000, Chemical and isotopical characterization  
999 of fluid manifestations of Ischia Island (Italy).: *J.Volcanol.Geoth.Res.*, v. 99, p. 151-178.
- 1000 Inguaggiato, S. and Rizzo, A., 2004, Dissolved helium isotope ratios in ground-waters: a new  
1001 technique based on gas-water re-equilibration and its application to Stromboli volcanic system:  
1002 *Applied Geochem.*, v. 19, p. 665-673.

1003 Inguaggiato, S., Martin-Del Pozzo, A. L., Aguayo, A., Capasso, G., and Favara, R., 2005,  
1004 Isotopic, chemical and dissolved gas constraints on spring water from Popocatepetl (Mexico):  
1005 evidence of gas-water interaction magmatic component and shallow fluids:  
1006 *J.Volcanol.Geoth.Res.*, v. 141, p. 91-108.

1007 Inguaggiato, S; Hidalgo S.; Beate B; and Bourquin J. (2010) Geochemical and isotopic  
1008 characterization of volcanic and geothermal fluids discharged from the Ecuadorian volcanic arc  
1009 *GEOFLUIDS* 10, 525–541- 2010

1010 Inguaggiato S, Vita F, Rouwet D, Bobrowski N, Morici S, Sollami A (2011)- Geochemical  
1011 evidence of the renewal of volcanic activity inferred from CO<sub>2</sub> soil and SO<sub>2</sub> plume fluxes: the  
1012 2007 Stromboli eruption (Italy) *Bullettin of Volcanology* 2011, Vol 73, Number 4, Pages 443-  
1013 456

1014 Inguaggiato S., M.P. Jacome Paz, A. Mazot, H. Delgado Granados, C. Inguaggiato, F. Vita  
1015 (2013) CO<sub>2</sub> output discharged from Stromboli Island (Italy). *Chemical Geology* (2013)  
1016 <http://dx.doi.org/10.1016/j.chemgeo.2012.10.008>

1017 Inguaggiato, S., Vita, F., Cangemi, M., Mazot, A., Sollami, A., Calderone, L., ... & Paz, M. P. J.  
1018 (2017a). Stromboli volcanic activity variations inferred from observations of fluid geochemistry:  
1019 16 years of continuous monitoring of soil CO<sub>2</sub> fluxes (2000–2015). *Chemical Geology*, 469, 69-  
1020 84.

1021 Inguaggiato, C., Vita, F., Diliberto, I. S., & Calderone, L. (2017b). The role of the aquifer in soil  
1022 CO<sub>2</sub> degassing in volcanic peripheral areas: A case study of Stromboli Island (Italy). *Chemical*  
1023 *Geology*, 469, 110-116.

- 1024 Inguaggiato, S.; Diliberto, I.S.; Federico, C.; Paonita, A.; Vita, F. (2017). Review of the  
1025 evolution of geochemical monitoring, networks and methodologies applied to the volcanoes of  
1026 the Aeolian Arc (Italy). *Earth-Sci. Rev.* 2018, 176, 241–276 [10.1016/j.earscirev.2017.09.006](https://doi.org/10.1016/j.earscirev.2017.09.006)
- 1027 Inguaggiato S., Vita F., Cangemi M. and Calderone L. (2019) Increasing Summit Degassing at  
1028 the Stromboli Volcano and Relationships with Volcanic Activity (2016–2018). *Geosciences* 9,  
1029 176.
- 1030 Inguaggiato, S.; Vita, F.; Cangemi, M.; Calderone, L. Changes in CO<sub>2</sub> Soil Degassing Style as a  
1031 Possible Precursor to Volcanic Activity: The 2019 Case of Stromboli Paroxysmal Eruptions.  
1032 *Appl. Sci.* 2020, 10, 4757
- 1033 Inguaggiato, S.; Vita, F.; Cangemi, M.; Inguaggiato, C.; Calderone, L. (2021) The Monitoring of  
1034 CO<sub>2</sub> Soil Degassing as Indicator of Increasing Volcanic Activity: The Paroxysmal Activity at  
1035 Stromboli Volcano in 2019–2021. *Geosciences* 2021, 11, 169.  
1036 <https://doi.org/10.3390/geosciences11040169>
- 1037 Lages, J., Rizzo, A.L., Aiuppa, A., Robidoux, P., Aguilar, R., Apaza, F., Masias, P. (2021)  
1038 Crustal controls on light noble gas isotope variability along the Andean Volcanic Arc. *Geochem.*  
1039 *Persp. Let.* 19, 45–49| doi: [10.7185/geochemlet.2134](https://doi.org/10.7185/geochemlet.2134)
- 1040 Landi, P., Corsaro, R. A., Francalanci, L., Civetta, L., Miraglia, L. Pompilio, Tesoro, R., 2009.  
1041 Magma dynamics during the 2007 Stromboli eruption (Aeolian islands, Italy). *Mineralogy,*  
1042 *geochemistry and isotope data. J. Volcanol. Geother. Res.* 182, 255-268.
- 1043 Lénat, J.F., Bachélery, P., Peltier, A., (2012). The interplay between collapse structures,  
1044 hydrothermal systems, and magma intrusions: the case of the central area of Piton de la Fournaise  
1045 volcano. *Bull. Volcanol.* 74, 407–421. <https://doi.org/10.1007/s00445-011-0535-3>.

- 1046 Liotta M., Brusca L., Grassa F., Inguaggiato S., Longo M. and Madonia P. (2006) *Geochemistry*  
1047 of rainfall at Stromboli volcano (Aeolian Islands): Isotopic composition and plume-rain  
1048 interaction. *Geochem. Geophys. Geosyst.* 7.
- 1049 Lorenz, V. & Kurszlaukis, S., 2007. Root zone processes in the phreatomagmatic pipe  
1050 emplacement model and consequences for the evolution of maar-diatreme volcanoes, *J. Volc.*  
1051 *Geotherm. Res.*, 159(1–3), 4–32.
- 1052 Lupton, J., M. Lilley, D. Butterfield, L. Evans, R. Embley, G. Massoth, B. Christenson, K.-I.  
1053 Nakamura, and M. Schmidt (2008), Venting of a separate CO<sub>2</sub>-rich gas phase from submarine  
1054 arc volcanoes: Examples from the Mariana and Tonga-Kermadec arcs, *J. Geophys. Res.*, 113,  
1055 B08S12, doi:10.1029/2007JB005467.
- 1056 Madonia, P.; Campilongo, G.; Cangemi, M.; Carapezza, M.L.; Inguaggiato, S.; Ranaldi, M.;  
1057 Vita, F. Hydrogeological and Geochemical Characteristics of the Coastal Aquifer of Stromboli  
1058 Volcanic Island (Italy). *Water* 2021, 13, 417. <https://doi.org/10.3390/w13040417>
- 1059 Martelli, M., A.L., Rizzo, A., Renzulli, F., Ridolfi, I., Arienzo, A., Rosciglione (2014) Noble-gas  
1060 signature of magmas from a heterogeneous mantle wedge: The case of Stromboli volcano  
1061 (Aeolian Islands, Italy). *Chem. Geol.* 368, 39-53.
- 1062 Mauri, G., Saracco, G., Labazuy, P., Williams-Jones, G. (2018). Correlating hydrothermal  
1063 system dynamics and eruptive activity – A case-study of Piton de la Fournaise volcano, La  
1064 Réunion. *J. Volcanol. Geother. Res.* 363, 23-39.
- 1065 Métrich, N., Bertagnini, A., Di Muro, A., 2010. Conditions of magma storage, degassing and  
1066 ascent at Stromboli: new insights into the volcano plumbing system with inferences on the  
1067 eruptive dynamics. *J. Petrol.* 51, 603–626. doi: 10.1093-petrology-egp083.

1068 Métrich N, Bertagnini A and Pistolesi M (2021) Paroxysms at Stromboli Volcano (Italy):  
1069 Source, Genesis and Dynamics. *Front. Earth Sci.* 9:593339. doi: 10.3389/feart.2021.593339

1070 Morelli, C., Giese, P., Cassinis, R., Colombi, B., Guerra, I., Luongo, G., Scarascia, S., Schutte,  
1071 K.G., 1975. Crustal structure of Southern Italy. A seismic refraction profile between Puglia–  
1072 Calabria–Sicily. *Boll. Geofis. Teor. Appl.* 18, 183–210.

1073 Ohsawa, S., Kazahaya, K., Yasuhara, M., Kono, T., Kitaoka, K., Yusa, Y., & Yamaguchi, K.  
1074 (2002). Escape of volcanic gas into shallow groundwater systems at Unzen Volcano (Japan):  
1075 evidence from chemical and stable carbon isotope compositions of dissolved inorganic carbon.  
1076 *Limnology*, 3(3), 0169-0173.

1077 Osinski, G.R., Spray, J.G., Lee, P., 2001. Impact-induced hydrothermal activity within the  
1078 Haughton impact structure, arctic Canada: generation of a transient, warm, wet oasis. *Meteorit.*  
1079 *Planet. Sci.* 36 (5), 731–745.

1080 Panza, G.F., Peccerillo, A., Aoudia, A., Farina, B., 2007. Geophysical and petrological  
1081 modelling of the structure and composition of the crust and upper mantle in complex  
1082 geodynamic settings: the Tyrrhenian Sea and surroundings. *Earth Sci. Rev.* 80, 1–46.

1083 Paonita, A., M. Longo, S. Bellomo, W. D'Alessandro, L. Brusca (2016). Dissolved inert gases  
1084 (He, Ne and N<sub>2</sub>) as markers of groundwater flow and degassing areas at Mt Etna volcano (Italy)  
1085 *Chemical Geology* 443, 10–21 doi: 0.1016/j.chemgeo.2016.09.018

1086 Prano, V. Liotta M. (2018), Precisione e accuratezza nella determinazione dei costituenti  
1087 maggiori in soluzione acquosa mediante cromatografia ionica: stime per i cromatografi Dionex  
1088 ICS-1100 utilizzati presso la Sezione INGV di Palermo. INGV Technical Reports  
1089 <https://doi.org/10.13127/rpt/390>



- 1090 Revil, A., Linde, N., 2006. Chemico-electromechanical coupling in microporous media. *J.*  
1091 *Colloid Interface Sci.* 302, 682–694. doi:10.1016/j.jcis.2006.06.051.
- 1092 Revil, A., Finizola, A., Ricci, T., Delcher, E., Peltier, A., Barde-Cabusson, S., ... & Tsang Hin  
1093 Sun, E. (2011). Hydrogeology of Stromboli volcano, Aeolian Islands (Italy) from the  
1094 interpretation of resistivity tomograms, self-potential, soil temperature and soil CO<sub>2</sub>  
1095 concentration measurements. *Geophysical Journal International*, 186(3), 1078-1094.
- 1096 Rizzo, A., Aiuppa, A., Capasso, G., Grassa, F., Inguaggiato, S., Longo, M., & Carapezza, M. L.  
1097 (2008). The 5 April 2003 paroxysm at Stromboli: A review of geochemical observations. In  
1098 *Learning from Stromboli and its 2002-03 eruptive crisis*. American Geophysical Union.  
1099 Washington DC American Geophysical Union Geophysical Monograph Series, 182, 347-358.
- 1100 Rizzo A., Grassa F., Inguaggiato S., Liotta M., Longo M., Madonia P., Brusca L., Capasso G.,  
1101 Morici S., Rouwet D. and Vita F. (2009) Geochemical evaluation of observed changes in  
1102 volcanic activity during the 2007 eruption at Stromboli (Italy). *J. Volcanol. Geotherm. Res.* 182.
- 1103 Rizzo A L, Federico C, Inguaggiato S, Sollami A, Tantillo M, Vita F, Bellomo S, Longo M,  
1104 Grassa G, Liuzzo M (2015). The 2014 effusive eruption at Stromboli volcano (Italy): Inferences  
1105 from soil CO<sub>2</sub> flux and He-3/He-4 ratio in thermal waters. *GEOPHYSICAL RESEARCH*  
1106 *LETTERS*, vol. 42, p. 2235-2243, ISSN: 0094-8276, doi: 10.1002/2014GL062955
- 1107 Rizzo A. L., Caracausi A., Chavagnac V., Nomikou P., Polymenakou P., Mandalakis M.,  
1108 Kotoulas G., Magoulas A., Castillo A., Lampridou D. 2016a, Kolumbo submarine volcano  
1109 (Greece): An active window into the Aegean subduction system. *Sci. Rep.* 6, 28013; doi:  
1110 10.1038/srep28013
- 1111 Rizzo AL, Caracausi A, Chavagnac V, Nomikou P, Polymenakou PN, Mandalakis M, Kotoulas  
1112 G, Magoulas A, Castillo A, Lampridou D, Maruszczak N and Sonke JE (2019) Geochemistry of

- 1113 CO<sub>2</sub>-Rich Gases Venting From Submarine Volcanism: The Case of Kolumbo (Hellenic  
1114 Volcanic Arc, Greece). *Front. Earth Sci.* 7:60. doi: 10.3389/feart.2019.00060
- 1115 Rizzo A.L., Robidoux P., Aiuppa A., Di Piazza A. (2022). <sup>3</sup>He/<sup>4</sup>He signature of magmatic fluids  
1116 from Telica (Nicaragua) and Baru (Panama) volcanoes, Central American Volcanic Arc. *Appl.*  
1117 *Sci.*, 12, 4241. <https://doi.org/10.3390/app12094241>
- 1118 Robidoux, P., Rizzo, A., Aguilera, F., Aiuppa, A., Artale, M., Liuzzo, M., Nazzari, M., Zummo,  
1119 F. (2020). Petrological and noble gas features of Lascar and Lastarria volcanoes (Chile):  
1120 Inferences on plumbing systems and mantle characteristics. *LITHOS*, ISSN: 0024-4937, doi:  
1121 10.1016/j.lithos.2020.105615
- 1122 Rosi, M., A. Bertagnini, and P. Landi (2000), Onset of the persistent activity at Stromboli  
1123 volcano (Italy), *Bull. Volcanol.*, 62, 294–300.
- 1124 Sander, R. (2015). Compilation of Henry's law constants (version 4.0) for water as solvent.  
1125 *Atmos. Chem. Phys.*, 15, 4399–4981.
- 1126 Schiavi, F., Kobayashi, K., Nakamura, E., Tiepolo, M., Vannucci, R., 2012. Trace element and  
1127 Pb–B–Li isotope systematics of olivine-hosted melt inclusions: insights into source  
1128 metasomatism beneath Stromboli (southern Italy). *Contrib. Mineral. Petrol.* 163, 1011–1031.
- 1129 Simmons, S. F., & Christenson, B. W. (1994). Origins of calcite in a boiling geothermal system.  
1130 *American journal of science*, 294(3), 361-400.
- 1131 Singaraja C., Chidambaram S. and Jacob N. (2018) A study on the influence of tides on the  
1132 water table conditions of the shallow coastal aquifers. *Appl. Water Sci.* 8, 11.
- 1133 Taran, Y., Kalacheva, E., Inguaggiato, S., Cardellini, C., Karpov, G. (2017). Hydrothermal  
1134 systems of the Karymsky Volcanic Centre, Kamchatka: Geochemistry, time evolution and solute  
1135 fluxes. *J. Volcanol. Geotherm. Res.* 346, 28-39.

- 1136 Tommasini, S., Heumann, A., Avanzinelli, R., Francalanci, L., 2007. The fate of high-angle  
1137 dipping slabs in the subduction factory: an integrated trace element and radiogenic isotope (U,  
1138 Th, Sr, Nd, Pb) study of Stromboli volcano, Aeolian Arc, Italy. *J. Petrol.* 48:2407–2430.  
1139 <http://dx.doi.org/10.1093/petrology/egm066>.
- 1140 Valsami-Jones, E., Baltatzis, E., Bailey, E. H., Boyce, A. J., Alexander, J. L., Magganas, A., ... &  
1141 Ragnarsdottir, K. V. (2005). The geochemistry of fluids from an active shallow submarine  
1142 hydrothermal system: Milos island, Hellenic Volcanic Arc. *Journal of Volcanology and*  
1143 *Geothermal Research*, 148(1-2), 130-151.
- 1144 Villasante-Marcos, V., Finizola, A., Abella, R., Barde-Cabusson, S., Blanco, M. J., Brenes, B., ...  
1145 & Trigo, P. (2014). Hydrothermal system of Central Tenerife volcanic complex, Canary Islands  
1146 (Spain), inferred from self-potential measurements. *Journal of volcanology and geothermal*  
1147 *research*, 272, 59-77.
- 1148 Vita, F., Inguaggiato, S., Capasso, G., Liotta, M., Rizzo, A. L., 2023. Chemical-physical  
1149 parameters, major, and minor elements composition of thermal waters from 8 wells in the  
1150 Stromboli aquifer (Italy), Version 1.0 [Dataset]. Interdisciplinary Earth Data Alliance (IEDA).  
1151 <https://doi.org/10.26022/IEDA/112932>.
- 1152 Weinstein, Y., 2007. A transition from strombolian to phreatomagmatic activity induced by a  
1153 lava flow damming water in a valley, *J. Volc. Geotherm. Res.*, 159(1–3), 267–284.
- 1154 Yamada, M., Ohsawa, S., Kazahaya, K., Yasuhara, M., Takahashi, H., Amita, K., ... &  
1155 Yoshikawa, S. (2011), Mixing of magmatic CO<sub>2</sub> into volcano groundwater flow at Aso volcano  
1156 assessed combining carbon and water stable isotopes, *Journal of Geochemical Exploration*,  
1157 *108(1)*, 81-87.
- 1158

1159 **Figure 1.** Location of sampling points and main regional faults N41°; N64° (Finizola et al.,  
 1160 2002). The map reference system is ETRS89/UTM 33 N. The red square marks the position of  
 1161 Stromboli Island in Southern Italy.

1162 **Figure 2.** Well data plotted on a chlorine (Cl) - sodium (Na) diagram. The mean amount-  
 1163 weighted composition of rainwater (Liotta et al. 2006) and dripping water from a cave in the  
 1164 neighborhood of Fulco well are also plotted.

1165 **Figure 3.** Diagram showing  $\delta D$  versus  $\delta^{18}O$  in the groundwater of Stromboli. The grey area  
 1166 defines the composition of the meteoric recharge (Liotta et al., 2006). The dashed lines are the  
 1167 Global Meteoric Water Line (GMWL) and the Eastern Mediterranean Meteoric Water Line  
 1168 (EMMWL) (Gat and Carmi, 1970). Dripping water at Fulco cave (FCDW) is also plotted as well  
 1169 as the Mediterranean seawater (SW) (Gat et al., 1996).

1170 **Figure 4.** Relative contents of He, CH<sub>4</sub>, and CO<sub>2</sub> (cc/L at STP). Curves 1, 2, and 3 represent the  
 1171 modeled composition of the dissolved gas, obtained by partial dissolution, in a shallow aquifer at  
 1172 40°C, of a gas having initial CH<sub>4</sub>/CO<sub>2</sub> ratios of  $5 \cdot 10^{-5}$ ,  $1 \cdot 10^{-4}$  and  $2 \cdot 10^{-4}$  respectively, and  
 1173 He/CO<sub>2</sub> =  $2.4 \cdot 10^{-5}$ , hypothesized to be separated from an underlying boiling aquifer. The crosses  
 1174 on the red curves refer to different fractions of residual gas after dissolution ( $F_2$  in equation 2, see  
 1175 Appendix 1).

1176 **Figure 5.**  $\delta^{13}C_{CO_2}$  versus dissolved CO<sub>2</sub>. Values of  $\delta^{13}C_{CO_2}$  are computed from measured  $\delta^{13}C_{TDC}$   
 1177 (method given in the text).

1178 **Figure 6.**  $^4He/^{20}Ne$  vs  $^4He$  cc/L at STP in the thermal wells of Stromboli. Air Saturated Water  
 1179 (ASW) with  $^4He/^{20}Ne = 0.285$  and  $^4He = 4.55 \cdot 10^{-5}$  cc/L at STP is plotted for comparison.

1180 **Figure 7.**  $^4He/^{20}Ne$  vs  $^3He/^4He$  expressed as R/Ra. The two curves indicate mixing lines between  
 1181 an atmospheric component with  $^4He/^{20}Ne = 0.318$  and R/Ra=1 and two possible magmatic end  
 1182 members with  $^4He/^{20}Ne = 100$ , as observed in other analogous investigations (e.g., Rizzo et al.,  
 1183 2015, 2022; Robidoux et al., 2020; Lages et al., 2021), and 3.8-4.6 Ra that includes all the data  
 1184 variability observed in 2004-2018. The rectangle reports the maximum range of values measured  
 1185 in fluid inclusions from LP magma minerals (Martelli et al., 2014).

1186 **Figure 8.** Time series of R<sub>c</sub>/R<sub>a</sub> values measured in gases dissolved in the thermal waters of  
 1187 Stromboli. Red bars indicate the periods of lava effusion, the red symbol the paroxysmal  
 1188 explosion occurred on the 15 of March, 2007.

1189 **Figure 9.** Stromboli groundwater samples displayed on a plot of Cl against K. All the samples  
 1190 show enrichment in K compared to the seawater ratio. The mean amount-weighted composition  
 1191 of rainwater (Liotta et al. 2006) and dripping water (FCDW) from a cave in the neighborhood of  
 1192 Fulco well are also plotted.

1193 **Figure 10.** Stromboli groundwater samples displayed on a plot of Cl against total alkalinity.  
 1194 With the exception of Zurro and COA, samples exhibit a negative relationship between Cl and  
 1195 total alkalinity (see text for details).

1196 **Figure 11.** Chlorine versus dissolved He/CO<sub>2</sub> ratios in the wells COA, Limoneto, and Piscità.  
1197 Symbols as in Figure 2.

1198 **Figure 12.** Scatter plot of CH<sub>4</sub>/CO<sub>2</sub> versus He/CO<sub>2</sub> ratios measured in well waters. Gas  
1199 concentrations are expressed as cc/L at STP. Curves 1, 2, and 3 represent the modeled  
1200 composition of the dissolved gas, obtained by partial dissolution, in a shallow aquifer at 40°C, of  
1201 a gas having initial CH<sub>4</sub>/CO<sub>2</sub> ratios of 5·10<sup>-5</sup>, 1·10<sup>-4</sup> and 2·10<sup>-4</sup> respectively, and He/CO<sub>2</sub>= 2.4·10<sup>-5</sup>,  
1202 hypothesized to be separated from an underlying boiling aquifer. The crosses on the red curves  
1203 refer to different fractions of residual gas after dissolution (F<sub>2</sub> in equation 2, Appendix 1).  
1204 Colored lines represent the mixing between different end members (green crosses), marine or  
1205 meteoric in origin, characterized by different gas compositions. The composition of air-saturated  
1206 water (MW) and seawater (SW) at 15°C is plotted for comparison (ASW: CO<sub>2</sub>=0.38 cc/L,  
1207 He=4.5·10<sup>-5</sup> cc/L, CH<sub>4</sub>= 7.8·10<sup>-5</sup> cc/L at STP; ASSW: CO<sub>2</sub>=0.32 cc/L, He=3.8·10<sup>-5</sup> cc/L, CH<sub>4</sub>=  
1208 5.9·10<sup>-5</sup> cc/L at STP; Liotta and Martelli, 2012).

1209 **Figure 13.** a) Scatter plot of Cl versus CO<sub>2</sub> contents measured in well waters. Colored lines  
1210 represent the mixing between different end members, marine or meteoric in origin, characterized  
1211 by different CO<sub>2</sub> contents. The composition of air-saturated water (MW) and seawater (SW) is  
1212 plotted for comparison; b) scatter plot of Cl versus CH<sub>4</sub> contents measured in well waters. Green  
1213 lines represent the mixing between different end members, marine or meteoric in origin,  
1214 characterized by different CH<sub>4</sub> contents; c) scatter plot of Cl versus He contents measured in well  
1215 waters. Green lines represent the mixing between different end members, marine or meteoric in  
1216 origin, characterized by different He contents.

1217 **Figure 14.** Time trends of He (left axis) and Cl (right axis) in well Limoneto.

1218 **Figure 15.** Frequency and cumulative frequency distribution of <sup>3</sup>He/<sup>4</sup>He in Stromboli thermal  
1219 wells, based on 511 measurements carried out between 2004 and 2018. Considering the analysis  
1220 of the frequency of occurrence of Rc/Ra values over 14 years of monitoring and taking into  
1221 account the maximum value measured in fluid inclusions of LP minerals (Martelli et al., 2014),  
1222 the variability of Rc/Ra values is reported as a function of variable extents of mixing between  
1223 fluids degassed from an LP magma, having ratios as high as 4.6 Ra, and those from an HP  
1224 magma, supposed to have the lowest Rc/Ra values recorded in the time series.

1225 **Figure 16.** Interpretative model of the shallow thermal aquifer obtained by merging the  
1226 outcomes of Finizola et al. (2010), Revil et al. (2011), Madonia et al. (2021) and the elaborations  
1227 of the present work.

1228

## 1229 Appendix 1

### 1230 Chemical fractionation of gas as an effect of dissolution

1231 The chemical fractionation upon dissolution can be reliably modeled by a Rayleigh's type  
1232 process, according to the equation (Albarède, 1995; Capasso et al., 2005):

$$1233 \left( \frac{[G_1]}{[G_2]} \right)_{liq} = \frac{K_{H,2}}{K_{H,1}} \cdot \left( \frac{[G_1]}{[G_2]} \right)_{gas,i} \cdot F_2^{\left( \frac{K_{H,2}}{K_{H,1}} - 1 \right)} \quad (1)$$

1234 where G1 and G2 are two gas species, the subscripts liq and gas, i refer to the liquid and the  
1235 initial gas phase, respectively; F2 is the residual fraction of the gas species 2, KH is Henry's  
1236 constants of the two gas species.

1237 In the following, we compute the evolution of He/CO<sub>2</sub> and CH<sub>4</sub>/CO<sub>2</sub> ratios according to eq. 1,  
1238 by assuming He and CH<sub>4</sub> as species 1, and CO<sub>2</sub> as species 2, respectively. In Figure 4, the  
1239 theoretical composition of the dissolved gas, after the removal of an increasing amount of gas  
1240 upon dissolution in water, is plotted. The initial gas compositions (i.e.  $\left(\frac{[G_1]}{[G_2]}\right)_{gas,i}$ ) in equation 1  
1241 are selected to best fit the observed data. The different curves refer to three different initial  
1242 CH<sub>4</sub>/CO<sub>2</sub> ratios.

1243 The Henry's constants were computed at 40°C, and their values are 144000 and 50560 bar mol  
1244 mol<sup>-1</sup>, for He and CH<sub>4</sub>, respectively. The Kh computed for CO<sub>2</sub> (2263 bar mol mol<sup>-1</sup> at 40°C) is  
1245 reduced by the effect of CO<sub>2</sub> hydration, which depends also on pH and on the dissociation of  
1246 carbonic acid (see Capasso et al., 2005). The used value is 1440 bar mol mol<sup>-1</sup>, computed at pH =  
1247 6 and 40°C.

1248 As explained by Capasso et al. (2005), the retrieved initial He/CO<sub>2</sub> ratios ( $2 \cdot 10^{-5}$ ) are higher than  
1249 those measured on average in a fumarole sampled in the Pizzo area (SC5; Capasso et al., 2005)  
1250 and measured in fluid inclusions (Gennaro et al., 2017) (He/CO<sub>2</sub> ratio ranging from  $3 \cdot 10^{-6}$  to  $10^{-5}$ ),  
1251 and this implies a probable enrichment in He during the vapor separation from an underlying  
1252 biphasic aquifer, and particularly for a small fraction of separated gas. The modeled initial  
1253 CH<sub>4</sub>/CO<sub>2</sub> contents span from  $5 \cdot 10^{-5}$  to  $2 \cdot 10^{-4}$  and are higher than those measured in the SC5  
1254 fumarole (Carapezza and Federico, 2000; Capasso et al., 2005), suggesting a variable CH<sub>4</sub>  
1255 production in different portions of the hydrothermal aquifer or different periods, besides an  
1256 additional enrichment after vapor separation.

1257 Madonia et al. (2021) suggested the existence of a stratified (multilevel) hydrothermal aquifer,  
1258 with temperatures that could be progressively higher, in the deeper and inner parts of the island.  
1259 The hypothesized fractionation upon dissolution in the shallow aquifer would produce a  
1260 progressive enrichment in He and CH<sub>4</sub> and depletion of CO<sub>2</sub>, toward a gas composition, which in  
1261 the studied aquifer is characterized by He contents as high as  $2.5 \cdot 10^{-3}$  cc/L at STP and CO<sub>2</sub>  
1262 contents as low as 10 cc/L at STP.

1263